

Quantifying innate and adaptive immunity during influenza infection using sequential infection experiments and mathematical models

Proceedings of the Royal Society B

^{1,2}Ada W. C. Yan

³Sophie G. Zaloumis

³ Julie A. Simpson

^{1,3,4}James M. McCaw (corresponding)

¹School of Mathematics and Statistics, The University of Melbourne, VIC, Australia

²MRC Centre for Outbreak Analysis and Modelling, Department of Infectious Disease Epidemiology, School of Public Health, Imperial College London, London, UK

³Melbourne School of Population and Global Health, The University of Melbourne, VIC, Australia

⁴Modelling and Simulation, Infection and Immunity Theme, Murdoch Childrens Research Institute, The Royal Childrens Hospital, Parkville, VIC, Australia.

E-mail: jamesm@unimelb.edu.au

Abstract

Recent experiments where ferrets were exposed to two influenza strains within a short time have provided insight into the timing and contribution of each immune component to cross-protection. While mathematical models which capture the novel observations have been developed and analysed, they have many parameters and it is unclear whether the contributions of each immune component to cross-protection can be recovered from the data.

We show using Markov chain Monte Carlo methods that within a simulation estimation framework, a model fitted to sequential infection data accurately captures the timing and extent of cross-protection, and attributes such cross-protection to the correct broad immune components. In addition, sequential infection data enables recovery of the timing and role of each immune component in controlling a primary infection. A major limitation of previous studies using single infection data is that they have produced discrepant estimates of these quantities.

This evaluation demonstrates that sequential infection experiments provide richer information for quantifying the contribution of each immune component to cross-protection. This information enhances our understanding of the mechanisms underlying the control and resolution of infection, and generates new insight into how previous exposure influences the time course of a subsequent infection.

Keywords: influenza, viral dynamics, cross-immunity, simulation estimation, Markov chain Monte Carlo, mathematical model

1 Introduction

The influenza virus infects epithelial cells in the respiratory tract, causing respiratory symptoms such as coughing and sneezing, and systemic symptoms such as fever. Three main components of the immune response — innate, humoral adaptive and cellular adaptive immunity — work together to control an infection. The contribution of each major immune component to resolution of an infection has been established using experiments where various immune components are suppressed [18, 64, 32, 74, 37]. However, current mathematical models of influenza do not agree on the contribution of each immune component to resolution of an infection.

Discrepancies between these models regarding the contribution of each immune component to controlling infection were demonstrated in the study

by Dobrovolny et al. [18]. In this study, different components of the immune response were removed from eight existing models [4, 29, 55, 63, 27, 8, 47, 39]; the viral load was then compared to that observed in the aforementioned experiments where various immune components were suppressed. None of the reviewed models qualitatively reproduced all of the experimentally observed effects of removing innate, cellular adaptive and/or humoral adaptive immunity.

We hypothesise that the discrepancies between models arise because many models are only fit to viral load data from a single infection. Even a model without a time-dependent immune response can fit the viral load for a single infection well [4]; however, if data for multiple initial conditions are available, the viral load may have more features to distinguish between competing models [41, 1].

One way of altering the initial conditions is through a previous or ongoing infection. We previously conducted a series of experiments where ferrets were sequentially infected with two influenza strains [38]. These experiments demonstrated that a primary infection confers temporary immunity against a subsequent infection when a short time interval (1–14 days) separates exposures. This protection conveys information about the timing and strength of cross-immunity conferred by each immune component, whereby the immune response stimulated by one strain also protects against infection with another.

Few existing models were equipped to model interactions between influenza infections separated by such short times; hence, we constructed viral dynamics models to reproduce the qualitative observations of these experiments [12, 73]. The models can also reproduce observations from a range of experiments where immune components are suppressed [11]. However, because of the many parameters required for a model to describe all major immune components, it is unclear whether the quantitative contribution of each immune component to cross-protection can be recovered from sequential infection data.

Here, we conduct a simulation estimation study to determine the additional immunological information which can be obtained by fitting a viral dynamics model to sequential infection data, rather than to data from a single infection only. Section 2.1 provides an overview of the simulation estimation study, while the remainder of Section 2 details the methods used. The goodness of fit of the model to the generated data is demonstrated in Section 3.1. Section 3.2 then assesses whether key immunological quantities, such as the contributions of innate and adaptive immunity to cross-protection, can be accurately recovered from sequential infection data.

2 Materials and Methods

2.1 Overview of simulation estimation study

We use a simulation estimation study to determine whether key immunological quantities can be extracted from sequential infection data, and whether sequential infection data enables more accurate extraction of these quantities than single infection data. The quantities to be extracted are:

- the timing and extent of cross-protection;
- the cross-protection conferred by each immune component; and
- the timing and role of each component in controlling a primary infection.

The steps of the simulation estimation study are as follows:

1. Choose an influenza viral dynamics model (Section 2.2), and a set of ‘true’ parameters (Section 2.3).
2. Determine immunological quantities according to the model and ‘true’ parameters, by simulating the viral load using *in silico* experiments designed to extract these quantities (Section 2.3).
3. Using the above model and parameter values, generate a sequential infection data set where ferrets are exposed to two influenza strains, with intervals of 1, 3, 5, 7, 10 and 14 days between exposures; and a single infection data set where ferrets are exposed once only (Section 2.4).
4. Fit the model in step 1 to each data set in step 3 (Section 2.5), to obtain the joint posterior distribution of the parameters given the data set for each scenario.
5. Use the joint posterior distributions in step 4 to obtain the 95% prediction intervals for the same *in silico* experiments as step 2.
6. Compare the ‘true’ viral load trajectories in step 2 to the 95% prediction intervals in step 5.

2.2 The model

The viral dynamics model is based on a model we previously published [72]. It incorporates three major components of the immune response — innate, humoral adaptive and cellular adaptive.

Figure 1 shows a compartmental diagram of the model. The equations are given by Eq. A.1 in Appendix A.

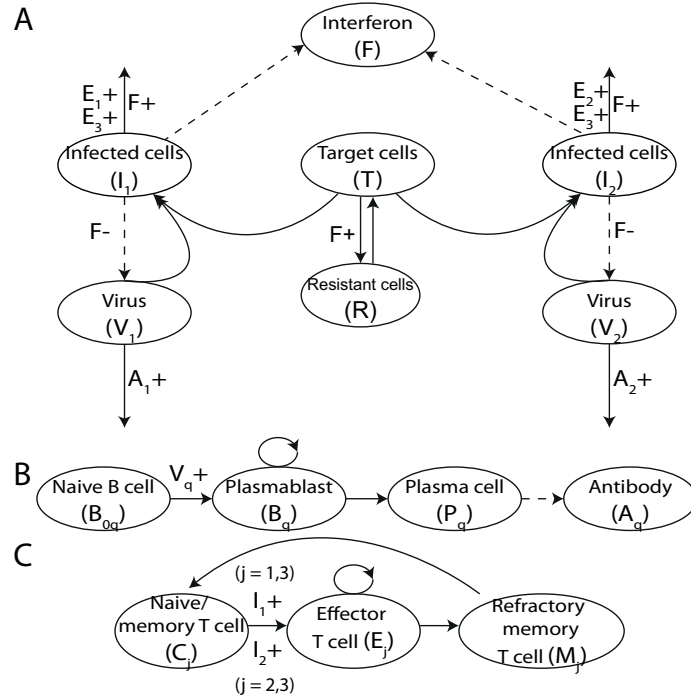


Figure 1: *The within-host influenza model illustrated using two strains and three $CD8^+$ T cell pools.* (A) Viral dynamics and innate immune response; (B) humoral adaptive immune response for virus strains $q = 1, 2$; (C) cellular adaptive immune response for T cell pools $j = 1, 2, 3$. Solid arrows indicate transitions between compartments or death (shown only for immune-enhanced death processes); dashed arrows indicate production; plus signs indicate an increased transition rate due to the indicated compartment. In this example, cells infected with influenza strain 1 stimulate naive $CD8^+$ T cells in pools 1 and 3, and are cleared by effector $CD8^+$ T cells in these pools. Cells infected with influenza strain 2 stimulate naive $CD8^+$ T cells in pools 2 and 3, and are cleared by effector $CD8^+$ T cells in these pools.

Virions of strain q (V_q) bind to target cells (T) to infect them; infected cells (I_q) produce virions of the same strain; and infected cells and virions

both decay at a constant rate. Target cells also regrow, with an imposed carrying capacity.

Innate immunity is mediated through type I interferon (F), the production of which is stimulated by cells infected with either strain. Three effects of type I interferon are modelled:

- rendering target cells temporarily resistant to infection ($T \rightarrow R$);
- decreasing the production rate of virions from infected cells; and
- increasing the decay rate of infected cells.

The humoral adaptive immune response is mediated by strain-specific antibodies (A_q), which bind to virions and neutralise them. A series of events triggered by the strain-specific stimulation of naive B cells (B_{0q}) eventually lead to antibody production.

The cellular adaptive immune response is mediated by J pools of effector CD8⁺ T cells E_j . Infected cells stimulate the differentiation of effector CD8⁺ T cells from their naive counterparts; effector CD8⁺ T cells then increase the death rate of infected cells. Some effector CD8⁺ T cells remain after a primary infection as memory CD8⁺ T cells, which can be re-stimulated to become effector CD8⁺ T cells upon challenge. The stimulation of naive CD8⁺ T cells is strain-specific, although there may not be a one-to-one correspondence between virus strains and T cell pools. Figure 1 depicts the situation where naive CD8⁺ T cell pools 1 and 3 are stimulated by cells infected with strain 1, and naive CD8⁺ T cell pools 2 and 3 are stimulated by cells infected with strain 2. The clearance of infected cells by effector CD8⁺ T cells is similarly strain-specific.

2.3 Parameter selection

The ‘true’ parameter values chosen to generate the synthetic data are given in Tables A.1–A.4 in Section A.4. The parameters are assumed to be identical between the two strains, except for the parameters governing cross-reactivity in the cellular adaptive immune response. The parameter values are chosen to conform to the following criteria.

2.3.1 The qualitative behaviour of the model for a single infection

The model should produce a viral load trajectory that can be split into exponential growth, plateau and decay phases, similar to the model by Cao et al. [11]. This behaviour matches experimental results by Laurie et al. [38].

2.3.2 The timing and extent of cross-protection between strains

The qualitative behaviour of the model for sequential infections should match the experiments by Laurie et al. [38] when infection is with influenza strains of different types (A and B).

- For short inter-exposure intervals (1–5 days), infection with the challenge virus is delayed;
- for long inter-exposure intervals (7–14 days), infection with the challenge virus is unaffected.

In this case, we hypothesise that the degree of cross-reactivity in the cellular adaptive immune response to the two strains is low, as suggested by murine studies [20, 7]. Appendix C presents results for an additional set of parameters where the degree of cross-reactivity in the cellular adaptive immune response is high. These results are quantitatively similar to those in the main text, and further support the conclusions herein that sequential infection data provides richer information about both cross-protection and resolution of a single infection.

2.3.3 The immune components governing cross-immunity

In our model, the cross-protection between strains is mediated through three direct effects of the primary infection:

- target cell depletion due to the infection and subsequent death of cells;
- innate immunity; and
- cross-reactive cellular adaptive immunity.

These mechanisms each lower the effective reproduction number of the challenge strain, but to different extents depending on parameter values. Note that because the model includes target cell regrowth, infection with the challenge virus can become established despite target cell depletion due to the death of infected cells.

We can determine the extent to which each immune component mediates cross-protection for a particular set of parameters using *in silico* experiments simulated from models where the mechanisms mediating cross-protection are restricted. To do so, we modify the models such that either

- cross-protection is only mediated by cellular adaptive immunity, and not target cell depletion or innate immunity (model XC); or

- cross-protection is mediated by target cell depletion and/or innate immunity, but not cellular adaptive immunity (model XIT).

These models are illustrated in Section A.2. The section also contains the changed equations (relative to Eq. A.1) for model XC, and the changed parameter values for model XIT. The cross-protection observed when model XC is used with a particular set of parameter values is the cross-protection mediated by cellular adaptive immunity in the baseline model for the same parameter values. Similarly, the cross-protection observed when model XIT is used with a particular set of parameter values is the cross-protection mediated by target cell depletion and/or innate immunity in the baseline model for the same parameter values.

Note that for a single infection, model XC and model XIT generate the same viral load as the baseline model.

The parameters for generating the synthetic data are chosen such that cross-protection for short inter-exposure intervals is mainly due to innate immunity rather than target cell depletion or cellular adaptive immunity; the simulation estimation study will explore whether the relative contributions of these three components can be recovered from the data.

2.3.4 The timing and role of each immune component in controlling a single infection

The parameters are chosen such that the qualitative behaviour of the model for a single infection when immune components are suppressed is consistent with experimental data [64, 32, 74, 37]. This behaviour reflects the timing and role of each immune component in controlling a single infection:

- when the innate adaptive immune response is absent ($F \rightarrow 0$), the peak viral load increases [64];
- when the humoral adaptive immune response is absent ($A \rightarrow 0$), the viral load rebounds [32];
- when the cellular adaptive immune response is absent ($E \rightarrow 0$), resolution of the infection is delayed [74]; and
- when both arms of the adaptive immune response are absent ($A, E \rightarrow 0$), chronic infection ensues [37].

2.4 Generation of synthetic data

The model and the chosen ‘true’ parameters are used to generate synthetic data where ferrets are exposed to two influenza strains sequentially, with intervals of 1, 3, 5, 7, 10 and 14 days between exposures. In addition, thirteen ferrets are exposed to a single influenza strain only. The sequential infection data set consists of the viral load for the six sequential infection ferrets and one single infection ferret; the single infection data set consists of the viral load for the thirteen single infection ferrets. The number of single infection ferrets is chosen such that the number of exposures to influenza virus is the same in each data set, and so the number of data points is roughly the same. Measurement error is added to the data, as described in Section A.3. Note that simulations where immune components are suppressed, and where the mechanisms mediating cross-protection are restricted, are not included in the synthetic data; we will investigate whether the fitted model can reproduce these predictions despite the lack of direct information.

2.5 Estimation of model parameters from synthetic data

We use Markov chain Monte Carlo methods to sample the joint posterior distribution for the parameters given each data set, as detailed in Section A.5. The prior distributions are chosen to encompass parameter estimates in previous studies, and are chosen to be wide such that the posterior distributions are chiefly driven by the synthetic data rather than the prior. Details of the prior distribution are given in Section A.4.2.

3 Results

3.1 Goodness of fit of the model to the generated synthetic data

First, we establish that the model recovers the viral load when fitted to either single infection or sequential infection data. Figure 2a presents prediction intervals for the viral load for a single infection, for both the model fitted to sequential infection data and the model fitted to single infection data. The prediction intervals include the ‘true’ viral load, confirming the goodness of fit of the model when fitted to either data set.

To be precise, the blue and green areas are the 95% prediction intervals for the viral load generated using the joint posterior distribution for the

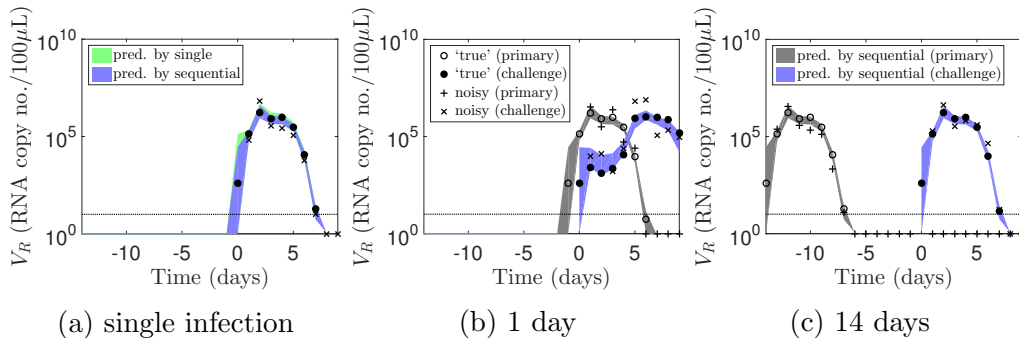


Figure 2: *The generated data and prediction intervals for the viral load, for the models fitted to the sequential and single infection data sets. The prediction intervals include the ‘true’ viral load, confirming the goodness of fit of the model when fitted to either data set. (a) The dots show the viral load for a single infection simulated using the model and the ‘true’ parameters. The viral load with measurement noise is shown as crosses. Note that the dots and crosses are the same for either the single infection or the sequential infection data (the crosses show the viral load for the one single infection ferret which overlaps between the two data sets). The blue and green areas are the 95% prediction intervals for the viral load generated using the joint posterior distribution for the parameters, obtained by fitting the model to the sequential infection and single infection data respectively. (b–c) The viral load is simulated for sequential infections with the labelled inter-exposure interval. The open and closed dots show the viral load for a primary and challenge infection respectively. The grey and blue areas show the 95% prediction intervals for the primary and challenge viral load respectively, predicted by the model fitted to sequential infection data. The horizontal line indicates the observation threshold; observations below this threshold are plotted below this line.*

parameters, obtained by fitting the model to the sequential infection and single infection data respectively; this data is shown as crosses. Both shaded areas include the viral load simulated using the ‘true’ parameters, shown as dots. This consistency indicates that the model fits the data well.

Figures 2b and 2c show the viral load for different inter-exposure intervals, predicted by the model fitted to sequential infection data. The grey and blue areas, which show the 95% prediction intervals for the primary and challenge viral load respectively, demonstrate a good fit of the model to the data.

An examination of the marginal posterior distributions for the parameters (Section B.3) shows that for some parameters, the marginal posterior distributions accurately recover the true values used to generate the data. For other parameters, the marginal distributions contain little information. In some cases, the distributions even exhibit bias. These results indicate that an evaluation of the model fit to the experimental data should not be limited to examining the marginal posterior distributions of the parameters; indeed, such a focus would overlook valuable information contained in the highly correlated joint posterior distribution about the role of each immune component in controlling infection. Thus, we proceed to use *in silico* experiments to extract immunological quantities from the joint posterior distribution.

The sequential infection viral load for the complete set of inter-exposure intervals used in the experiments by Laurie et al. [38], and the viral load for the remaining single infection ferrets, are shown in Section B.1.

3.2 Recovering immunological quantities

To determine whether immunological quantities can be recovered from a fitted model, we compare model behaviour for the ‘true’ parameters to that of the fitted model. Because a primary infection can greatly affect a challenge infection, but not vice versa, we focus on the behaviour of the challenge infection.

3.2.1 Determining the timing and extent of cross-protection between strains

The fact that the model fitted to sequential infection data recovers the viral load for different inter-exposure intervals (as shown in Fig. 2b–c) suggests that it accurately captures the timing and extent of cross-protection between strains. We test whether the model fitted to single infection data can also predict the viral load for these inter-exposure intervals.

Figure 3 presents a comparison of the predictive abilities of the models fitted to the two data sets. Figures 3a–b show that, unlike the predictions

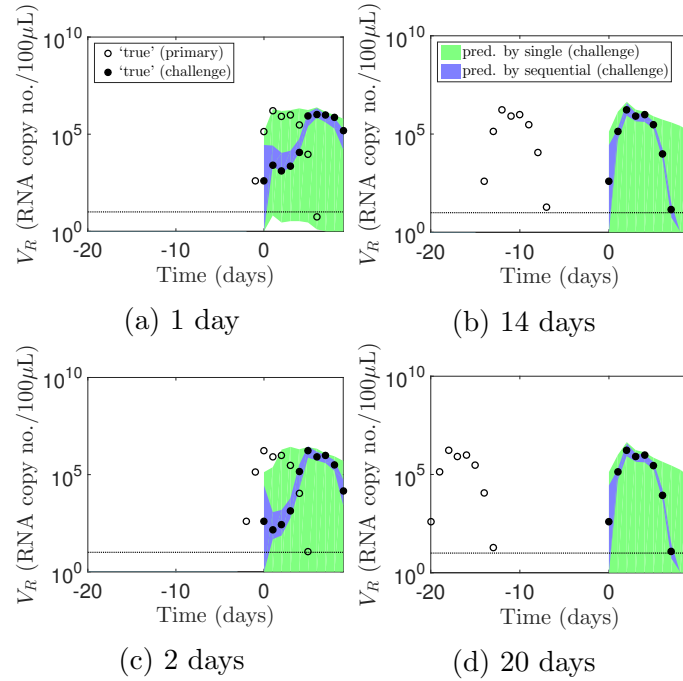


Figure 3: *A comparison of the abilities of the models fitted to the two data sets to predict the outcomes of sequential infection experiments. A model fitted to sequential infection data can predict outcomes of further sequential infection experiments using the same strains, while a model fitted to single infection data cannot predict sequential infection experiment outcomes. The dots show the viral load for inter-exposure intervals of 1, 14, 2 and 20 days, simulated using the ‘true’ parameters (shown without measurement noise). The shaded areas show the 95% prediction intervals for the viral load of the challenge strain (without measurement noise) for these inter-exposure intervals. The colours and markers are as per Fig. 2. Note that data for inter-exposure intervals of 1 and 14 days were present in the sequential infection data set, but data for inter-exposure intervals of 2 and 20 days were absent.*

by the model fitted to sequential infection data (blue), predictions by the model fitted to single infection data (green) do not agree well with the ‘true’ viral load. This finding demonstrates the value of fitting a model to sequential infection data. Details of extending the model fitted to single infection data to two strains, to enable prediction of sequential infection experiment outcomes, are given in Section A.6.

We additionally test whether a model fitted to sequential infection data can predict the viral load for inter-exposure intervals not included in the data. Successful prediction would provide further evidence that this model accurately captures the timing and extent of cross-protection.

Figures 3c–d show prediction intervals for the viral load for inter-exposure intervals of 2 days and 20 days respectively. The blue areas, which correspond to the model fitted to sequential infection data, accurately predict the viral load for the challenge strain. Significantly, the fitted model is not only able to predict infection outcomes for inter-exposure intervals between those included in the original data (1, 3, 5, 7, 10 and 14 days), but also inter-exposure intervals outside this range. Note that the model was not re-fitted to the viral load for the new inter-exposure intervals. On the other hand, the green areas, which correspond to the model fitted to single infection data, continue to predict the viral load with poor precision.

These results indicate that a model fitted to sequential infection data captures the timing and extent of cross-protection, while a model fitted to single infection data does not.

3.2.2 Determining the cross-protection conferred by each immune component

Section 2.3.3 outlined how the baseline model in Fig. 1 can be modified such that either only cellular adaptive immunity mediates cross-protection (model XC), or only target cell depletion and/or innate immunity mediates cross-protection (model XIT).

First we demonstrate, using the ‘true’ parameter values, how the modified models can be used to extract the contributions to cross-protection by either cellular adaptive immunity, or target cell depletion/innate immunity. Figure 4 shows predictions of the challenge viral load using models XC and XIT for the ‘true’ parameter values (black dots). Comparing these predictions to the viral load in the absence of the primary virus (red dots), we see a large deviation for model XIT at a one-day inter-exposure interval (Fig. 4b). This suppression indicates that at a one-day inter-exposure interval, target cell depletion and/or innate immunity mediate cross-protection. By contrast, the overlap between the remaining trajectories indicates that for a

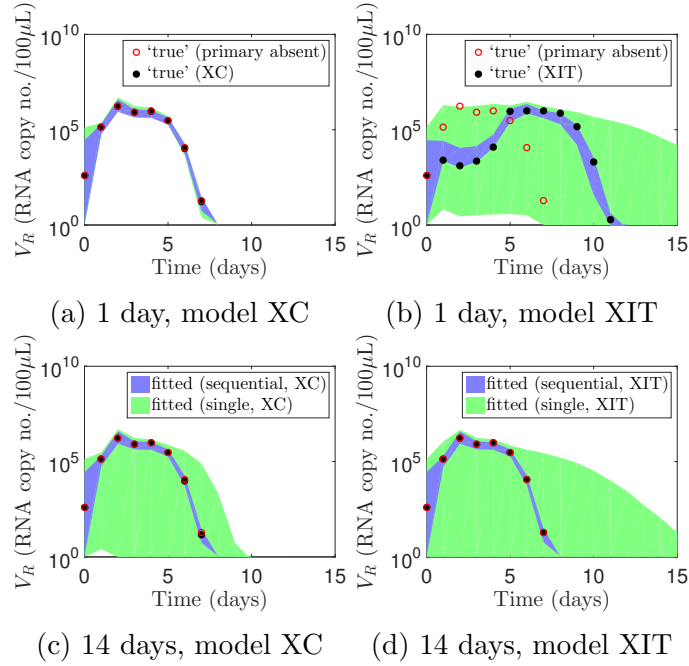


Figure 4: A comparison of the abilities of the models fitted to the two data sets to predict the challenge viral load when the mechanisms mediating cross-protection are restricted. Comparing the challenge viral load for the ‘true’ parameter values when the mechanisms mediating cross-protection are restricted (models XC and XIT, black dots) to the viral load in the absence of the primary virus (red dots) shows that at a one-day inter-exposure interval, target cell depletion and/or innate immunity mediate cross-protection, whereas cellular adaptive immunity does little to mediate cross-protection; at a 14-day inter-exposure interval, none of the components lead to significant cross-protection. The model fitted to sequential infection data accurately predicts the challenge outcomes (blue, 95% prediction intervals shown), while the model fitted to single infection data does not consistently do so (green).

one-day inter-exposure interval, cellular adaptive immunity contributes little to cross-protection (Fig. 4a); and that for a 14-day inter-exposure interval, little cross-protection is observed due to any component (Figs. 4c–d).

Now that we have demonstrated how the modified models can be used to extract the contributions to cross-protection, we compare the predictive abilities of the models fitted to the two data sets. The blue areas show that the model fitted to sequential infection data accurately predicts the challenge outcomes for models XC and XIT, over a range of inter-exposure intervals. This result demonstrates that the model fitted to sequential infection data captures the cross-protection conferred by either cellular adaptive immunity, or a combination of target cell depletion and innate immunity. On the other hand, the green areas show that the model fitted to single infection data does not always accurately predict the challenge viral load for models XC and XIT.

In detail, the model fitted to single infection data does accurately recover the viral load for a one-day inter-exposure interval for model XC (Fig. 4a). Hence, it correctly determines that cellular adaptive immunity confers little cross-protection at a short inter-exposure interval. However, it does not accurately recover the viral load for model XIT (Fig. 4b), so it does not consistently capture the cross-protection due to target cell depletion and/or innate immunity. For a 14-day inter-exposure interval, the model fitted to single infection data predicts that either cellular adaptive immunity (Fig. 4c), or a combination of target cell depletion and innate immunity (Fig. 4d), could confer cross-protection. This is inconsistent with model behaviour for the ‘true’ parameters.

While the combined contribution to cross-protection by target cell depletion and innate immunity can be extracted from sequential infection data, Section B.4 shows that the individual contributions to cross-protection by these two components cannot be reliably disentangled. Section B.5 shows that the contributions to cross-protection by each of the three innate immune mechanisms in the model also cannot be reliably extracted.

Section B.6 shows that a model fitted to sequential infection data accurately recovers the initial growth rate of the challenge virus for different inter-exposure intervals, for both the baseline model and models XC and XIT. This accurate estimation of the initial growth rate enables the fitted model to recover the timing and extent of cross-protection overall, as well as the contributions of cellular adaptive immunity and target cell depletion/innate immunity to this cross-protection.

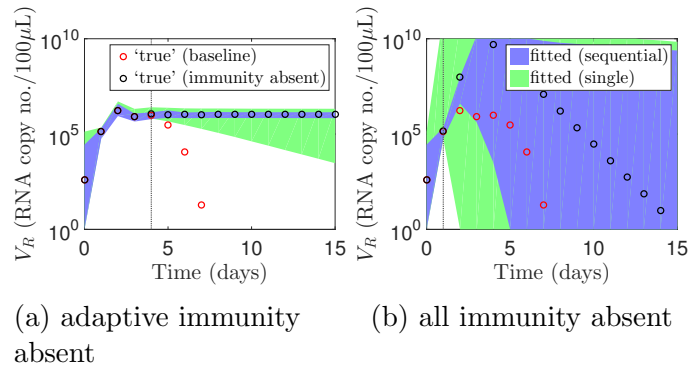


Figure 5: A comparison of the abilities of the models fitted to the two data sets to predict the viral load for a single infection when various immune components are absent. The vertical lines indicate, for the ‘true’ parameter values, the times at which (a) adaptive immunity and (b) innate immunity take effect. These are determined by when the viral load for the baseline model (black dots) deviates from the viral load when (a) adaptive immunity and (b) both innate and adaptive immunity are absent (red dots). The model fitted to sequential infection data recovers both of these times (95% prediction intervals for the viral load shown in blue), while the model fitted to single infection data (green) recovers the timing of adaptive immunity only. In addition, the prediction intervals for the model fitted to sequential infection data are tighter.

3.2.3 Determining the timing and role of each immune component in controlling a single infection

Figure 5 compares the abilities of the models fitted to the two data sets to predict the viral load for a single infection when various immune components are absent. The model fitted to sequential infection data predicts the viral load more accurately than the model fitted to single infection data.

Figure 5a shows that both the model fitted to sequential infection data and the model fitted to single infection data accurately capture the timing of adaptive immunity by recovering the time at which the viral load when adaptive immunity is absent (black dots) deviates from the baseline model (red dots); this time is indicated by the vertical line. However, only the model fitted to sequential infection data predicts correctly that the infection does not resolve in the absence of adaptive immunity. The model fitted to single infection data does not consistently predict this outcome.

Figure 5b shows that the model fitted to sequential infection data recovers the time at which the viral load deviates from the baseline model when both

innate and adaptive immunity are absent, whereas the model fitted to single infection data predicts that the viral load in the absence of the immune response may deviate from the baseline model much earlier. Neither model accurately predicts how the infection resolves in the absence of the immune response; however, the prediction intervals for the model fitted to sequential infection data are tighter, and the peak viral load is consistently predicted to be higher than in the baseline model.

In the absence of the immune response, the infection resolves due to target cell depletion only. The lack of predictive ability indicates that the models fitted to either data set lack information on how target cells would become depleted, and how this depletion would affect the viral load, in the absence of the immune response. One is thus cautioned against using parameter values from a model fitted to data in immunocompetent hosts to make predictions in situations where target cells may become severely depleted, such as if individuals are immunocompromised.

Results when the humoral and cellular adaptive immune response are separately absent are shown in Section B.7.

4 Discussion

4.1 Findings of the simulation estimation study

Three main results summarise the contributions of this study.

The first finding is that within the simulation estimation study framework, a model fitted to sequential infection data can predict outcomes of further sequential infection experiments using the same strains (Section 3.2.1). Significantly, this result shows that such a model correctly elucidates the timing and extent of cross-protection. By contrast, accurate recovery of these quantities is not possible with single infection data.

The second finding is that a model fitted to sequential infection data accurately recovers the viral load when the mechanisms mediating cross-protection are restricted (Section 3.2.2). This result implies that the model accurately determines the cross-protection due to cellular adaptive immunity, and the combined cross-protection by target cell depletion and innate immunity.

The last finding is that a model fitted to sequential infection data captures the timing of innate and adaptive immunity during a single infection, and can thus predict the outcomes of some *in silico* experiments where immune components are removed (Section 3.2.3). This finding shows that the model provides information not only on protection against subsequent infection, but

also on control of a primary infection.

We note that repeating the entire procedure with different noisy data sets (with the same ‘true’ parameters) does not change these findings (data and analysis not shown).

Collectively, the above findings strongly suggest that it will be possible to extract key immunological quantities by fitting the model to real experimental data — the fitted model will have both explanatory and predictive ability. Importantly, the sequential infection study design [38] provides a richer source of information for quantifying the extent of each immune component in controlling infection.

4.2 Limitations of sequential infection experiments identified by the study

This study has highlighted some limitations in quantifying this model of the immune response (Fig. 1) using sequential infection experiments.

Firstly, even under simulation estimation study conditions, the contributions of target cell depletion and innate immunity to protection against a subsequent infection cannot be reliably disentangled (Section B.4). The roles of the three proposed innate immune mechanisms [12] also cannot be distinguished (Section B.5).

Secondly, the study has shown that the effects of removing humoral adaptive immunity and cellular adaptive immunity in a primary infection cannot be disentangled (Section B.7).

Thirdly, the fitted model does not accurately recover the trajectories for compartments which are not measured, such as the number of target cells, the number of infected cells, and the infectious viral load (Section B.8). Although the main aim of the study is to quantify the contributions of innate and adaptive immunity to protection against a subsequent infection, the values of some compartments may be of intrinsic value; for example, the number of dead cells is an indication of disease severity.

It is possible that these quantities could be identified by incorporating other available data from the sequential infection experiments [38]. Such data includes infectious viral load measurements for single infection ferrets, and serological responses and cytokine levels at limited time points. One could use a further simulation estimation study to assess the additional information gained by fitting the model to this type of data.

Furthermore, new experiments could be conducted to improve parameter estimates and quantify the roles of immune components more accurately. Previous studies have measured viral decay rates *in vitro* and incorporated

these estimates into model fitting [58, 54]. As certain immune components are active *in vitro* — such as the inhibition of viral production from infected cells [49] — *in vitro* studies may offer a way to directly measure the time course of these mechanisms.

4.3 Future work and concluding summary

The experiments by Laurie et al. [38] were designed to further understanding of the mechanisms driving temporary immunity conferred by a primary infection against a subsequent infection. By conducting a simulation estimation study, significant progress has been made in ensuring that results are interpreted appropriately when models are fitted to experimental data to test our hypotheses. However, a simulation estimation study alone does not enable biological claims to be made about the validity of the final model, or the properties of the strains in the experiments. Our study has also not yet quantified the contribution of each immune component to control of an infection. Accordingly, a priority is to fit the model to the experimental data by Laurie et al. [38].

We have demonstrated that relative to single infection experiments, the sequential infection study design provides richer information for quantifying the contribution of each immune component to cross-protection on short timescales, leading to new insight into how previous exposure influences the time course of a subsequent infection. Further, data from sequential infection experiments provides improved power to discriminate between existing models for a primary infection, enhancing our understanding of the mechanisms underlying the control and resolution of infection.

Data accessibility

Code to generate all figures in this study is available at https://bitbucket.org/ada_yan/sim_est_immunity.

Authors' contributions

All authors conceived the study. A. W. C. Y. and J. M. M. developed the model used in the study. A. W. C. Y. performed the study and analysed the results, with input from S. G. Z., J. A. S. and J. M. M. All authors drafted the manuscript and approved the final version.

Funding

A. W. C. Y. is supported by an Australian Postgraduate Award (now Australian Government Research Training Program Scholarship), an Albert Shimmins Postgraduate Writing-up Award, and a Wellcome Trust Collaborator Award (UK, grant 200187/Z/15/Z). S. G. Z. is funded by an Australian Research Council (ARC) Discovery Early Career Researcher Award (DECRA) Fellowship (grant 170100785). J. A. S. is supported by a National Health and Medical Research Council (NHMRC) Senior Research Fellowship (grant 1104975). This research was supported by the ARC (grant DP170103076) and the NHMRC Centre of Research Excellence (grant 1058804). Computational support for this research was provided by Melbourne Bioinformatics at the University of Melbourne (grant VR0274), and the National eResearch Collaboration Tools and Resources (NeCTAR) Project.

Competing interests

We declare we have no competing interests.

Acknowledgements

We acknowledge helpful discussions with Pengxing Cao, Alexander E. Zarebski and Patricia T. Campbell.

Appendices

Contents

A	Detailed methods	23
A.1	Detailed description of the viral dynamics model	23
A.2	Detailed description of models XC and XIT	27
A.3	Observation model	30
A.4	Parameters and prior distributions	31
A.5	Model fitting methods	37
A.6	Extending the model fitted to single infection data to two strains	39
B	Additional results	40
B.1	Generated synthetic data	40
B.2	Convergence testing	42
B.3	Marginal posterior distributions	46
B.4	Distinguishing between target cell depletion and innate immunity	55
B.5	Distinguishing between mechanisms of the innate immune response	57
B.6	Estimating the initial growth rate of the second virus for different inter-exposure intervals	62
B.7	Determining the timing and role of humoral and cellular adaptive immunity in controlling a single infection	66
B.8	Predicting the trajectory of compartments other than the viral load	67
C	Additional results for a sequential infection, high cross-reactivity data set	69
C.1	The sequential infection, high cross-reactivity data set	69
C.2	Results	69

A Detailed methods

A.1 Detailed description of the viral dynamics model

The model equations are given by

$$\frac{dT}{dt} = g(T + R) \left(1 - \frac{T + R + \sum_{q=1}^Q I_q}{T_0} \right) - \sum_{q=1}^Q \beta_q V_q T + \rho R - \bar{\phi} \bar{F} T, \quad q = 1, \dots, Q, \quad (\text{A.1a})$$

$$\frac{dI_q}{dt} = \beta_q V_q T - \left(\delta_{I_q} + \bar{\kappa}_{Fq} \bar{F} + \sum_{j=1}^J \bar{\kappa}_{Ejq} \bar{E}_j \right) I_q, \quad q = 1, \dots, Q, \quad (\text{A.1b})$$

$$\frac{dV_q}{dt} = \frac{p_{Vq}}{1 + \bar{s}_q \bar{F}} I_q - (\delta_{Vq} + \bar{\kappa}_{Aq} \bar{A}_q + \beta_q T) V_q, \quad (\text{A.1c})$$

$$\frac{dV_{Rq}}{dt} = \frac{p_{Vq} p_{Rq} \alpha_q}{1 + \bar{s}_q \bar{F}} I_q - \delta_{V_{Rq}} V_{Rq} - \alpha_q \beta_q T V_q, \quad (\text{A.1d})$$

$$\frac{dR}{dt} = \bar{\phi} \bar{F} T - \rho R, \quad (\text{A.1e})$$

$$\frac{d\bar{F}}{dt} = \sum_{q=1}^Q \bar{p}_{Fq} I_q - \delta_F \bar{F}, \quad (\text{A.1f})$$

$$\frac{d\bar{B}_{0q}}{dt} = - \frac{V_{Rq}}{k_{Bq} + V_{Rq}} \beta_{Bq} \bar{B}_{0q}, \quad (\text{A.1g})$$

$$\frac{d\bar{B}_{1q}}{dt} = \frac{V_{Rq}}{k_{Bq} + V_{Rq}} \beta_{Bq} \bar{B}_{0q} - \frac{n_{Bq} \bar{B}_{1q}}{\tau_{Bq}} - \delta_{Bq} \bar{B}_{1q}, \quad (\text{A.1h})$$

$$\frac{d\bar{B}_{iq}}{dt} = \frac{n_{Bq} (2\bar{B}_{i-1,q} - \bar{B}_{iq})}{\tau_{Bq}} - \delta_{Bq} \bar{B}_{iq}, \quad i = 2, \dots, n_B, \quad (\text{A.1i})$$

$$\frac{d\bar{P}_q}{dt} = \frac{2n_{Bq} \bar{B}_{n_B,q}}{\tau_{Bq}} - \delta_{Bq} \bar{P}_q, \quad (\text{A.1j})$$

$$\frac{d\bar{A}_q}{dt} = \bar{P}_q - \delta_{Aq} \bar{A}_q, \quad (\text{A.1k})$$

$$\frac{d\bar{C}_j}{dt} = \frac{\bar{M}_j}{\tau_{Mj}} - \frac{\sum_{q=1}^Q I_q / k_{Cjq}}{1 + \sum_{q=1}^Q I_q / k_{Cjq}} \beta_{Cj} \bar{C}_j, \quad (\text{A.1l})$$

$$\frac{d\bar{E}_{1j}}{dt} = \frac{\sum_{q=1}^Q I_q / k_{Cjq}}{1 + \sum_{q=1}^Q I_q / k_{Cjq}} \beta_{Cj} \bar{C}_j - \left(\frac{n_{Ej}}{\tau_{Ej}} + \delta_{Ej} \right) \bar{E}_{1j}, \quad (\text{A.1m})$$

$$\frac{d\bar{E}_{ij}}{dt} = \frac{n_{Ej} (2\bar{E}_{i-1,j} - \bar{E}_{ij})}{\tau_{Ej}} - \delta_{Ej} \bar{E}_{ij}, \quad i = 2, \dots, n_E - 1, \quad (\text{A.1n})$$

$$\frac{d\bar{E}_{n_{Ej}}}{dt} = \frac{2n_{Ej} \bar{E}_{n_E-1,j}}{\tau_{Ej}} - \delta_{Ej} \bar{E}_{n_{Ej}}, \quad 23 \quad (\text{A.1o})$$

$$\bar{E}_j = \sum_{i=1}^{n_E} \bar{E}_{ij}, \quad (\text{A.1p})$$

$$\frac{d\bar{M}_j}{dt} = \epsilon_j \delta_{Ej} \bar{E}_{n_{Ej}} - \delta_{Ej} \bar{M}_j - \frac{\bar{M}_j}{\tau_{Mj}}. \quad (\text{A.1q})$$

We model infection by Q influenza strains, the innate and humoral adaptive immune response to those strains, and the cellular adaptive immune response to J epitopes across the Q strains.

The dynamics of infection (Fig. 1a in the main text) are described by Eqs. A.1a–A.1d. When target cells (T) are infected by virions of strain q (V_q), they become infected cells (I_q) which produce virions of the same strain. Both infected cells and virions decay at a constant rate, in addition to infected cell death mediated by natural killer cells and effector CD8⁺ T cells, and virion neutralisation due to antibodies.

The compartment V_q refers to the number of infectious virions in the host; however, an infected cell produces both infectious and non-infectious virions, the latter of which arise due to defects introduced during the viral replication process [52, 43]. Moreover, in the experiments conducted by Laurie et al. [38], the total viral load, rather than the number of infectious virions, is measured. An additional complication is that, rather than the absolute number of virions, the total viral load is measured in terms of its concentration in nasal wash. Hence, we incorporate the total viral load into the model, by introducing the following constants (adapted from Petrie et al. [57]):

- p_R , the ratio of total to infectious virions produced by an infected cell;
- α , the conversion factor from the total viral load concentration in nasal wash to the total number of virions in the respiratory tract (i.e. the RNA copy number/100 μ L which corresponds to one virion in the respiratory tract);
- γ , the initial ratio of total to infectious virions; and
- δ_{V_R} , the decay rate of the total number of virions.

Moreover, the decay rate of infectious virions δ_V is now interpreted as the rate at which infectious virions become non-infectious. The dynamics for the total virion concentration V_R are then described by Eq. A.1d. The last term in this equation reflects that only infectious virions can infect cells. Note that neutralisation by antibodies is absent from this equation (c.f. Eq. A.1c), reflecting that antibodies only render infectious virions non-infectious.

The innate immune response (Eqs. A.1e–A.1f, Fig. 1a in the main text) is mediated by type I interferon \bar{F} , which is produced in proportion to the number of infected cells of each strain at a rate \bar{p}_F , and decays at a rate δ_F . Note that because we only incorporate measurements of the total viral load V_{Rq} , some compartments and parameters are rescaled to decrease the number

of non-identifiable parameters; these scaled compartments and parameters are denoted by an overset bar (such as \bar{F}). Three effects of type I interferon are modelled.

1. Target cells are rendered temporarily resistant to infection. Target cells become resistant cells (R) at a rate proportional to both the number of target cells and the amount of interferon, with a rate constant $\bar{\phi}$. Resistant cells then return to their susceptible state at a rate ρ .
2. The production rate of virions from cells infected with strain q decreases by the factor $1 + \bar{s}_q \bar{F}$.
3. The decay rate of cells infected with strain q increases due to clearance by natural killer cells (an additional term $\bar{\kappa}_{Fq} I_q \bar{F}$). Natural killer cells are not modelled explicitly; rather, their number is assumed to be in proportion to type I interferon.

In addition, we model the regrowth of target cells as being proportional to both the number of uninfected cells ($T + R$) and the proportion of dead cells $1 - (T + R + \sum_{q=1}^Q I_q)/T_0$ (the model assumes that the total number of cells is constant). The first term models the proliferation of healthy cells, while the second term imposes a carrying capacity of T_0 . Modelling the regrowth of target cells enables their numbers to be restored when a long time interval separates exposures to two strains.

The model also captures the role of antibodies (\bar{A}_q), responsible for strain-specific viral clearance and induction of long-term sterilising immunity (Fig. 1b in the main text). We assume that any cross-reactive humoral immunity between the strains plays a subdominant part in the immune response [68, 26], such that there is a one-to-one correspondence between antibodies and the strains upon which they act. The equations which describe the production of antibodies are given by Eqs. A.1g–A.1k.

The stimulation of naive B cells (\bar{B}_{0q}) by both infectious and non-infectious virions (V_{Rq}) takes the form of a saturating function, as shown in Eq. A.1g. Once stimulated, naive B cells become plasmablasts (\bar{B}_{iq} where i denotes the stage of plasmablast) [48], as shown in Eq. A.1h. In Eqs. A.1h and A.1i, the plasmablasts undergo programmed proliferation for time τ_{Bq} , passing through n_{Bq} divisions/stages, until reaching the terminal stage – plasma cells (\bar{P}_q). Plasma cells (\bar{P}_q) produce antibodies (\bar{A}_q) which bind to virions and neutralise them. Plasmablasts can also produce antibodies, but at a lower rate [48], which we neglect in our model.

The cellular adaptive immune response (Fig. 1c in the main text), whereby effector CD8⁺ T cells accelerate the decay of infected cells, is described in

Eqs. A.1l–A.1q. We assume that there are $J = 3$ pools of naive CD8⁺ T cells, and that each of these recognises a single viral epitope, although cells infected with different strains can present the same epitope.

Epitopes are presented to CD8⁺ T cells by MHC class I molecules on the surface of either directly infected cells or on the surface of dendritic cells that have taken up the antigen and cross-presented it. Under a common modelling assumption (see e.g. Chao et al. [14]) that both direct presentation and cross-presentation are proportional to the number of infected cells, the model need not explicitly model cross-presentation.

Naive CD8⁺ T cell pool j (\bar{C}_j) is stimulated by interaction with the peptide-MHC complexes, as shown in Eq. A.1l; the stimulation function is a saturating function, such that k_{Cjq} is the number of cells infected with strain q required for (direct- and cross-) presentation of epitopes which yields half-maximal stimulation of the cellular adaptive immune response [17, 16, 14]. Once stimulated, naive CD8⁺ T cells divide to become effector CD8⁺ T cells of the first stage (\bar{E}_{1j}), as shown in Eq. A.1m; the effector cells then undergo programmed proliferation [34, 66, 71] for time τ_{Ej} , passing through n_{Ej} divisions, as shown in Eqs. A.1m, A.1n and A.1o. The subscript i denotes the stage of effector CD8⁺ T cell (1 to n_{Ej}).

When effector CD8⁺ T cells reach their last stage (the dynamics of which are described by Eq. A.1o), they no longer divide; instead, some fraction ϵ_j survive to become memory CD8⁺ T cells (\bar{M}_j). These memory CD8⁺ T cells are refractory in the sense that they cannot be restimulated for some time [35], which we model as exponentially distributed with mean τ_{Mj} . After this time, the memory CD8⁺ T cells can be restimulated. We assume that the properties of these memory CD8⁺ T cells are identical to those of naive CD8⁺ T cells, so we combine them into a single compartment \bar{C}_j . Upon restimulation, memory CD8⁺ T cells once again become effector CD8⁺ T cells \bar{E}_j .

The compartments whose values at the time of exposure to the first strain are estimated are T , the number of target cells; and V , the number of infectious virions. The initial concentration of total virus in nasal wash is then $V_R(0) = \gamma\alpha V_0$. The initial values of \bar{B}_{0q} and \bar{C}_j are normalised to 1. All other initial values are zero.

Instead of fitting the infectivity (β) and the production rate of infectious virions from an infected cell (p_V), we fit the basic reproduction number R_0 (Eq. A.2) and the initial viral load growth rate r (Eq. A.4), as we hypothesise that these are more intimately linked to features of the viral load curve.

The basic reproduction number R_0 is either the mean number of secondary infected cells due to (the virions produced by) a single infected cell, or the mean number of secondary virions produced by an initial virion through

the possibility of infecting a cell. (The two definitions yield the same value.) The expression for R_0 is

$$R_0 = \frac{\beta T_0 p_V}{(\delta_V + \beta T_0) \delta_I}, \quad (\text{A.2})$$

and is the same as that for a model without a time-dependent immune response [6].

The initial growth phase of the viral load trajectory can be approximated by

$$V = V_0 \exp(rt) \quad (\text{A.3})$$

where r is the Malthusian parameter. Arenas et al. [3] has shown using a simulation estimation study that this parameter is well estimated even when only viral load data is available.

The expression for r , derived by linearising Eq. A.1 around the disease-free equilibrium [53], is

$$r = -\frac{\delta_V + \beta T_0 + \delta_I}{2} + \frac{\sqrt{(\delta_I - \delta_V - \beta T_0)^2 + 4\beta T_0 p_V}}{2}. \quad (\text{A.4})$$

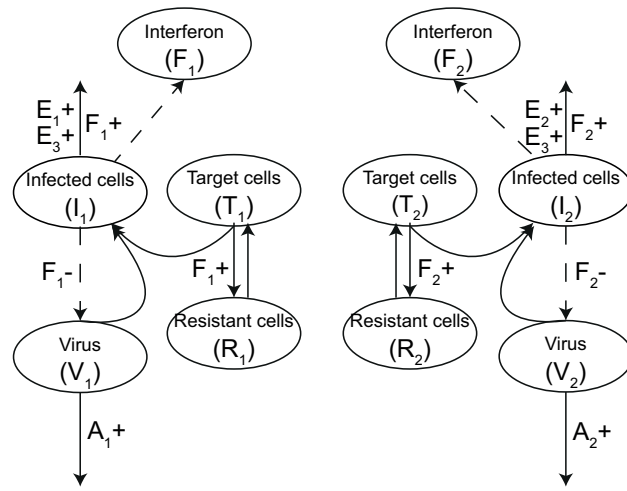
A.2 Detailed description of models XC and XIT

Section 2.3.3 in the main text asserted that for a given set of parameters, the contributions to cross-protection by cellular adaptive immunity, and that by target cell depletion/innate immunity, can be disentangled by modifying the baseline model such that either

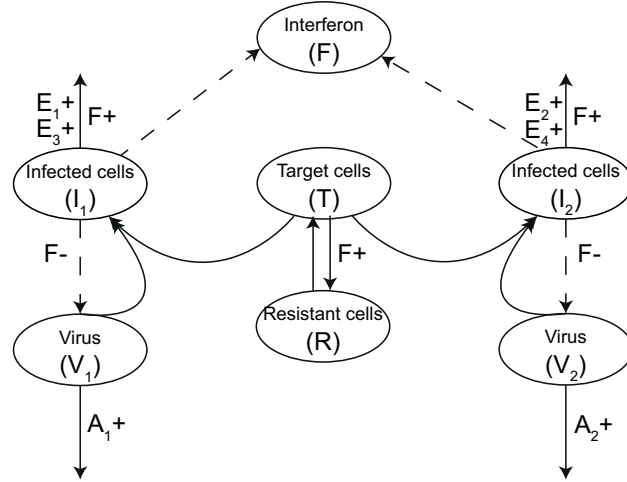
- cross-protection is only mediated by cellular adaptive immunity, and not target cell depletion or innate immunity (model XC); or
- cross-protection is mediated by target cell depletion and/or innate immunity, but not cellular adaptive immunity (model XIT).

These models are illustrated in Fig. A.1.

To explain model XC in detail (Fig. A.1a), type I interferon F_q are now strain-specific. Cells infected with strain q induce the production of interferon specific to that strain. The effects of interferon F_q — rendering target cells temporarily resistant to infection; lowering the production rate of virions; and increasing the death rate of cells — only apply to strain q . In addition, each strain now targets a separate pool of uninfected cells; the size of each target cell pool is T_0 (identical for both strains). This alternative model is



(a) model XC



(b) model XIT

Figure A.1: (a) A model where cross-protection is only mediated by cellular adaptive immunity (model XC). (b) A model where cross-protection is only mediated by target cell depletion and/or innate immunity (model XIT).

not meant to reflect a biologically realistic situation; however, it enables *in silico* thought experiments to determine, for a given set of parameters, the contribution of each immune component to cross-protection.

Explicitly, the changed equations (relative to Eq. A.1) for model XC are given by

$$\frac{dT_q}{dt} = g(T_q + R_q) \left(1 - \frac{T_q + R_q + I_q}{T_0} \right) - \beta_q T_q V_q - \bar{\phi}_q \bar{F}_q T_q + \rho_q R_q, \quad q = 1, \dots, Q, \quad (\text{A.5a})$$

$$\frac{dI_q}{dt} = \beta_q V_q T_q - \left(\delta_{I_q} + \bar{\kappa}_{F_q} \bar{F}_q + \sum_{j=1}^J \bar{\kappa}_{E_{jq}} \bar{E}_j \right) I_q, \quad (\text{A.5b})$$

$$\frac{dV_q}{dt} = \frac{pV_q}{1 + \bar{s}_q \bar{F}_q} I_q - [\delta_{V_q} + \bar{\kappa}_{A_q} \bar{A}_q + \beta_q T_q] V_q, \quad (\text{A.5c})$$

$$\frac{dV_{Rq}}{dt} = \frac{pV_q p_{Rq} \alpha_q}{1 + \bar{s}_q \bar{F}_q} I_q - \delta_{V_{Rq}} V_{Rq} - \alpha_q \beta_q T_q V_q, \quad (\text{A.5d})$$

$$\frac{dR_q}{dt} = \bar{\phi}_q \bar{F}_q T_q - \rho_q R_q, \quad (\text{A.5e})$$

$$\frac{d\bar{F}_q}{dt} = \bar{p}_{F_q} I_q - \delta_{F_q} \bar{F}_q. \quad (\text{A.5f})$$

The parameters which are newly strain-specific in model XC, such as $\bar{\phi}_q$, have identical values for each strain, which are the previously fitted values. The equations for \bar{B}_{iq} , \bar{P}_q , \bar{A}_q , \bar{C}_j , \bar{E}_{ij} and \bar{M}_j remain unchanged.

In the model where cross-protection is mediated by target cell depletion and/or innate immunity, but not cellular adaptive immunity (model XIT, Fig. A.1b), the cellular adaptive immune response is no longer cross-reactive. The model is altered from the original such that the number of T cell pools is $J = 4$. T cell pools 3 and 4 have the same parameters as pool 3 in the original model, but T cell pool 3 is stimulated by, and targets, cells infected with strain 1 only, while T cell pool 4 is stimulated by, and targets, cells infected with strain 2 only. (Explicitly, the cross-reactivity parameters for T cell pools 3 and 4 are $k_{C31} = k_{C42}$ equal to $k_{C31} = k_{C32}$ in the original model; $k_{C32} = k_{C41} = \infty$; $\bar{\kappa}_{E31} = \bar{\kappa}_{E42}$ equal to $\bar{\kappa}_{E31} = \bar{\kappa}_{E32}$ in the original model; and $\bar{\kappa}_{E32} = \bar{\kappa}_{E42} = 0$.) The cross-reactivity parameters for pools 1 and 2 remain the same.

A.3 Observation model

The measured viral load y_{qfk} for each virus $q = 1, 2, \dots, Q$, ferret $f = 1, 2, \dots, F$ and measuring time point t_{qfk} where $k = 1, 2, \dots, K_{qf}$ is given by

$$y_{qfk} = \begin{cases} V_{Rq}(t_{qfk}, u_f, \boldsymbol{\beta}) 10^{e_{qfk}} & \text{when } V_{Rq}(t_{qfk}, u_f, \boldsymbol{\beta}) 10^{e_{qfk}} \geq \Theta \\ 0 & \text{otherwise} \end{cases} \quad (\text{A.6a})$$

where $e_{qfk} \stackrel{i.i.d.}{\sim} \mathcal{N}(0, \sigma)$. (A.6b)

$\boldsymbol{\beta}$ is a vector of parameter values, u_f is an input scalar indicating the inter-exposure interval for ferret f , e_{qfk} is the measurement error, and Θ is a detection threshold. $V_{Rq}(t_{qfk}, \mathbf{u}_f, \boldsymbol{\beta})$ is the solution to Eq. A.1 for the V_{Rq} compartment at time t_{qfk} for the given parameter values and inter-exposure intervals. Θ takes the value 10 RNA copies/100 μ L in the experiments by Laurie et al. [38]. A measured viral load of 0 denotes that the viral load is below the detection threshold.

Therefore the likelihood of the model given the data is

$$P(\mathbf{y}|\boldsymbol{\theta}) = \prod_{q=1}^Q \prod_{f=1}^F \prod_{k=1}^{K_{qf}} P(y_{qfk}|\boldsymbol{\theta}) \quad \text{where} \quad (\text{A.7a})$$

$$P(y_{qfk}|\boldsymbol{\theta}) = \begin{cases} \frac{1}{\sqrt{2\sigma^2\pi}} \exp \left\{ -\frac{[\log_{10} y_{qfk} - \log_{10} V_{Rq}(t_{qfk}, u_f, \boldsymbol{\beta})]^2}{2\sigma^2} \right\} & \text{if } y_{qfk} \geq \Theta, \\ \int_0^{\Theta} \frac{1}{\sqrt{2\sigma^2\pi}} \exp \left\{ -\frac{[\log_{10} x - \log_{10} V_{Rq}(t_{qfk}, u_f, \boldsymbol{\beta})]^2}{2\sigma^2} \right\} dx & \text{if } y_{qfk} = 0, \\ 0 & \text{otherwise.} \end{cases} \quad (\text{A.7b})$$

In the second line of Eq. A.7b, the likelihood when the data is below the detection threshold is obtained by integrating the probability density function from 0 to the detection threshold, i.e. treating the data below the threshold as censored [2]. The vector $\boldsymbol{\theta}$ contains the parameters $\boldsymbol{\beta}$, the inter-exposure intervals u_f , the time points t_{qfk} , and the measurement error σ .

A.4 Parameters and prior distributions

A.4.1 Parameters for generating synthetic data

The ‘true’ parameter values chosen to generate the synthetic data are given in Tables A.1–A.4. The parameters are assumed to be identical between the two strains, except for the parameters governing cross-reactivity in the cellular adaptive immune response. The parameter values are chosen according to the criteria in Section 2.3 in the main text.

A.4.2 Prior distributions for model fitting

We fix two parameters — the number of plasmablast division cycles (n_B) and the number of effector CD8⁺ T cell division cycles (n_E) — to be 5 [42, 67] and 20 [66] respectively. For the remaining parameters, the joint prior distribution reflects the range of values found in the literature.

We begin with a uniform distribution in parameter space whose bounds along each dimension are given in Tables A.1–A.4. Note that parameter estimation is performed in a parameter space where all parameters except for the measurement error σ are log transformed. Then, we exclude regions of parameter space where the parameters $\log_{10} \beta$ and $\log_{10} p_V$, which are not directly estimated but are instead recovered from Eqs. A.2 and A.4, are outside the bounds given in Table A.1.

The priors are deliberately chosen to be wide because previous parameter estimates come from a range of experimental systems, and parameters with similar physical definitions can vary in value depending on the model used. The bounds for viral replication parameters are based on those by Petrie et al. [56] where the equivalent parameters exist. Otherwise, where multiple estimates exist in the literature (as cited in the tables), the bounds are chosen to encompass all of them. Where we can only find a single estimate, bounds around that estimate spanning at least an order of magnitude are chosen (unless the parameter is a pure rate parameter, as discussed shortly). Where no estimate was found in the literature, we choose a value based on the criteria outlined in Section 2.3 in the main text, and assign very wide bounds spanning much more than one order of magnitude around this value. In general, the bounds for pure rate parameters (those with units day^{-1} only) can be chosen to be narrower as the order of magnitude of the rate at which these processes occur is known, whereas bounds for parameters such as R_0 are much wider.

Furthermore, for computational efficiency, some minimal constraints on the behaviour of the viral load and timing of various immune components are incorporated into the prior distribution. These constraints are imposed

because parameter sets which generate ‘unreasonable’ viral load trajectories for a single infection cause large delays in numerical integration of the two-strain differential equations. The criteria by which these parameter sets are excluded are much less stringent than those used to select the parameter set with which to generate the synthetic data. They are that for a single infection,

- the total viral load rises by at least one order of magnitude during infection;
- the total viral load peaks 0–7 days post-exposure;
- the humoral adaptive immune response is not active too early (five days post-exposure, the neutralisation rate of virus by antibodies, $\bar{\kappa}_{A1}\bar{A}_1$, does not exceed 10^3 day^{-1}); and
- the cellular adaptive immune response is not active too early (five days post-exposure, the clearance rate of infected cells by effector CD8^+ T cells, $\sum_{j=1}^J \bar{\kappa}_{Ej1}\bar{E}_j$, does not exceed 10^3 day^{-1}).

If the viral load trajectory (in the absence of measurement noise) predicted by a parameter set does not fulfil all of these conditions, the value of the prior distribution is zero at that point in parameter space.

Parameter	Description	Value	Prior bounds	Units
$\log_{10} R_0$	basic reproduction number	$\log_{10} 4.9$	[0, 3] [28, 47, 55, 63, 65, 4]	
$\log_{10} r$	initial viral growth rate	$\log_{10} 6.56$	[0, 2] [28, 47, 55, 63, 65, 4]	day ⁻¹
$\log_{10} \delta_I$	infected cell decay rate	$\log_{10} 2$	[-1, 2] [56]	day ⁻¹
$\log_{10}(\delta_V - \delta_{VR})$	difference between infectious and total virion decay rates	$\log_{10} 2$	[-2, 2] [57]	day ⁻¹
$\log_{10} \delta_{VR}$	total virion decay rate	$\log_{10} 8$	[0, 2] [56]	day ⁻¹
$\log_{10} T_0$	initial number of target cells	$\log_{10}(7 \times 10^7)$	[7, 8] [57]	target cell
$\log_{10} g$	target cell regrowth rate	$\log_{10} 0.8$	[-10, 0.5] [50, 29, 39, 27, 8]	day ⁻¹
$\log_{10} p_R$	ratio of production of total to infectious virions	$\log_{10}(4 \times 10^4)$	[0, 6]	
$\log_{10} \alpha$	the number of RNA copies/100 μ L of nasal wash corresponding to one virion	$\log_{10} 0.01$	[-3, -1]	RNA copies/100 μ L virion ⁻¹
$\log_{10} \gamma$	the initial ratio of total to infectious virions	$\log_{10}(4 \times 10^4)$	[0, 5]	
$\log_{10} V_0$	the number of infectious virions upon exposure	$\log_{10} 1$	[0, 3]	virion
$\log_{10} \beta$	infectivity parameter	$\log_{10}(5 \times 10^{-7})$	[-12, -4] [56]	virion ⁻¹ day ⁻¹
$\log_{10} p_V$	production rate of infectious virions by infected cells	$\log_{10} 12.6$	[-6, 6] [56]	virion infected cell ⁻¹ day ⁻¹

Table A.1: Viral replication parameter values. β and p_V are not directly fitted, but their values as recovered from Eqs. A.2 and A.4 may not exceed the bounds given. The difference between the infectious and total virion decay rates $\delta_V - \delta_{VR}$, rather than the infectious virion decay rate δ_V , is fitted to ensure that the former quantity is positive, as infectious virions decay into non-infectious virions. Notes on biologically plausible ranges for the parameters p_R , α and γ are given in Section A.4.3.

Parameter	Description	Value	Prior bounds	Units
$\log_{10} \bar{p}_F$	normalised interferon production rate	$\log_{10} 1$	fixed	infected cell ⁻¹ day ⁻¹
$\log_{10} \bar{\delta}_F$	interferon decay rate	$\log_{10} 2$	$[-1, 2]$ [55, 8]	day ⁻¹
$\log_{10} \bar{\phi}$	(scaled) rate at which target cells become resistant to infection	$\log_{10}(3.3 \times 10^{-5})$	$[-10, 0]$ [63, 55]	day ⁻¹
$\log_{10} \rho$	rate at which resistant cells become susceptible to infection	$\log_{10} 2$	$[0, 2]$ [8, 27, 30, 13, 55]	day ⁻¹
$\log_{10} \bar{s}$	(scaled) factor by which the production rate of virions is decreased by type I interferon	5×10^{-4}	$[-10, 0]$	day ⁻¹
$\log_{10} \bar{\kappa}_F$	(scaled) clearance rate of infected cells by natural killer cells	$\log_{10}(2.5 \times 10^{-3})$	$[-10, 0]$ [55]	day ⁻¹

Table A.2: Innate immune response parameter values. Note that \bar{p}_F is equal to 1 by default because $\bar{p}_{Fi} := p_{Fi}/p_{F1}$, and we are assuming that all parameters are equal between strains.

Experiment	Parameter	Value	Prior bounds	units
Single infection	$\log_{10} k_{C11}$	5.05	$[-1, 10]$	infected cell
	$\log_{10} k_{C12}$	6	$[-1, 10]$	infected cell
	$\log_{10} \bar{\kappa}_{E11}$	$\log_{10} 0.0081$	$[-10, 3]$ [5]	day ⁻¹
Sequential infection	$\log_{10} k_{C11} = \log_{10} k_{C22}$	5.05	$[-1, 10]$	infected cell
	$k_{C12} = k_{C21}$	∞	fixed	infected cell
	$\log_{10} k_{C13} = \log_{10} k_{C23}$	6	$[-1, 10]$	infected cell
	$\log_{10} \bar{\kappa}_{E11}$	$\log_{10} 0.0081$	$[-10, 3]$ [5]	day ⁻¹

Table A.3: Values for the cross-reactivity parameters in the cellular adaptive immune response: the number of infected cells for half-maximal stimulation of naive/memory CD8⁺ T cells k_{Cjq} and the (scaled) clearance rate of infected cells by effector CD8⁺ T cells $\bar{\kappa}_{E11}$.

Parameter	Description	Value	Prior bounds	Units
$\log_{10} k_B$	concentration of viral RNA for half-maximal stimulation of naive B cells	$\log_{10}(2 \times 10^8)$	[1, 10]	RNA copy no./100 μ L
$\log_{10} \beta_B$	maximal stimulation rate of naive B cells	$\log_{10} 1$	[-5, 5]	day ⁻¹
$\log_{10} \tau_B$	total proliferation time of plasmablasts	$\log_{10} 4$	[0, 1] [42, 67]	day
$\log_{10} \bar{\kappa}_A$	(scaled) neutralisation rate of virions by antibodies	$\log_{10} 360$	[-10, 10] [47]	day ⁻¹
$\log_{10} \delta_A$	antibody decay rate	$\log_{10} 0.04$	[-2, -1] [8, 39]	day ⁻¹
$\log_{10} \delta_B$	plasmablast and plasma cell decay rate	$\log_{10} 0.11$	[-1, 0] [9, 48]	day ⁻¹
$\log_{10} \beta_C$	maximal stimulation rate of naive/memory CD8 ⁺ T cells	$\log_{10} 1$	[-5, 5]	day ⁻¹
$\log_{10} \tau_E$	total proliferation time of effector CD8 ⁺ T cells	$\log_{10} 5$	[0.5, 1] [40]	day
$\log_{10} \delta_E$	decay rate of effector CD8 ⁺ T cells	$\log_{10} 0.6$	[-1, 0] [70]	day ⁻¹
$\log_{10} \epsilon$	proportion of effector CD8 ⁺ T cells which become memory CD8 ⁺ T cells	$\log_{10} 0.02$	[-3, -1] [51, 17, 14]	
$\log_{10} \tau_M$	mean refractory time for memory CD8 ⁺ T cells	$\log_{10} 14$	[1, 1.5] [35]	day
σ	measurement error	0.5	[0, 2]	

Table A.4: Adaptive immune response and observation model parameter values.

A.4.3 Determining biologically plausible ranges for the parameters p_R , α and γ

First, we examine the parameter α . The concentration of virions in nasal wash is lower than the concentration of virions in the respiratory tract by a factor of $a = 1 - 100$ [28]. The volume of the ferret upper respiratory tract, which is assumed to be the site of infection, is approximately $v = 1\text{mL}$ [57], while the concentration of nasal wash is reported per $b = 0.1\text{mL}$ [38]. We assume that 1 RNA copy number corresponds to one (infectious or non-infectious) virion. Hence, the number of RNA copies/100 μL of nasal wash corresponding to one virion in the respiratory tract (α) is $(b/v)/a$. Based on the bounds for a and b , the bounds for α are then $[10^{-3}, 10^{-1}]$.

Next, we examine the parameter γ . Petrie et al. [56] use the bounds $[10^0, 10^5]$ to fit the initial ratio of total to infectious virions. These bounds are in units of RNA copy number/TCID₅₀ (f). These bounds are based on the variability across different inocula given to donor ferrets in the experiments by Butler et al. [10]; the study by Petrie et al. [56] analyses data from these experiments. However, in this study, γ is required to be in units of RNA copy number/virion, as we account for the loss of a single virion due to its infecting a target cell. Assays to measure the amount of infectious virus cannot measure the number of virions directly; hence, we must estimate the conversion factor between TCID₅₀ and virions (h). At the minimum, one virion is required to establish an infection; hence, the lower bound for the number of virions corresponding to 1 TCID₅₀ is 1 virion. Handel et al. [28] estimate that 1 TCID₅₀ corresponds to 1–100 virions, so the bounds for h are $[1, 100]$. Hence, the initial ratio of total to infectious virions in the respiratory tract in units of RNA copy number/virion (γ), which by definition has a lower bound of 1, is $\gamma = f/h$. Based on the bounds for f and h , the bounds for γ are then $[10^0, 10^5]$.

Lastly, we tackle the parameter p_R . Petrie et al. [56] use the bounds $[10^0, 10^6]$ to fit the ratio of production of total to infectious virions, in units of RNA copy number/TCID₅₀ (q). These bounds are based on the variability of this ratio in the data provided by Butler et al. [10]. The ratio of production of total to infectious virions in units of RNA copy number/virion (p_R), which also by definition has a lower bound of 1, is then $p_R = q/h$. Based on the bounds for h and q , the bounds for p_R are then $[10^0, 10^6]$.

A.5 Model fitting methods

Model fitting is conducted in Octave 3.8.2 [33]. To evaluate the likelihood, Eq. A.1 is solved using the CVODEs wrapper for MATLAB [69]. The wrap-

per uses the CVODE solvers developed by Cohen et al. [15]. Of the available solvers, a backward differentiation formula method in variable order, variable step, fixed leading coefficient form is chosen. Extinction is enforced by defining an infection to have resolved if both the number of infected cells and virions is below 0.1. The results of model fitting are visualised using MATLAB R2015b [44].

Fitting is conducted using the Metropolis algorithm [46, 45] embedded within a Gibbs sampler structure [24].

To assess convergence, three chains are run in parallel using different starting parameter values θ_0 drawn from the prior distribution. The procedure for determining the number of iterations for which to run the chains is as follows.

The three MCMC chains are truncated at k iterations, starting at $k = 10^4$. The first half of the chains are discarded as burn-in [21], and the 95% confidence interval for the potential scale reduction factor (PSRF) [23] for each parameter is calculated using the `gelman.diag` function in the `coda` package version 0.18-1 [59] in R version 3.3.2 [60]. If the upper bound of the 95% confidence interval for the PSRF is below 1.1 for all parameters, the chains are declared to have converged, and the process ends. All iterations of the three chains from $k/2 + 1$ onwards are then taken as draws from the joint posterior distribution. Otherwise, k is increased by 10^4 , and the process is repeated (with the original chains starting from the end of the calibrating stage). If the full number of iterations in the chain is reached and convergence still has not occurred, the chains are run for more iterations.

Once convergence is reached, the effective sample size is calculated for each chain (using the iterations which are kept following the burn-in process) using the `effectiveSize` function in the `coda` [59] package in R [60].

The marginal posterior distributions in this study are plotted as histograms using all samples from the MCMC chains (after burn-in), without thinning. When using the joint posterior distribution to make predictions, we use 10^4 parameter sets corresponding to uniformly spaced iterations in each of the chains.

For efficient mixing, the proposal distributions are tuned such that the proportion of accepted proposals is not too low or too high. To implement this tuning, a calibration period is introduced where the widths of the proposal distributions are adjusted. Initially, the proposal distribution for each parameter is set to be a uniform distribution centred at the current value of the parameter, of width equal to the bounds of the marginal prior distribution for that parameter. During calibration, the proposal distribution remains centred at the most current value of the parameter; only the width of each distribution changes. Every 100 iterations, the proportion of accep-

tance events during those 100 iterations for each parameter is checked. If the acceptance proportion is too low (a threshold is set at 0.3), the width of the proposal distribution is multiplied by 0.75; if the acceptance proportion is too high (above 0.5), the width of the proposal distribution is multiplied by 1.5. These thresholds are chosen because when each parameter is sampled in turn, for specific classes of likelihood functions, the optimal acceptance rate has been shown to be 0.44 [22]. However, we emphasise that tuning the acceptance rate merely enables convergence to occur within fewer iterations; attaining the optimal acceptance rate precisely is not essential. The calibration stage lasts for 10^4 iterations. The widths of the proposal distributions then stay fixed, and the initial 10^4 iterations are discarded.

For each of the three chains, parallel tempering (as developed by Geyer [25] and reviewed by Earl & Deem [19]) is implemented to improve exploration of parameter space. The number of iterations before testing whether to swap chains in the parallel tempering process is set to 10.

During the calibration period for the proposal distributions, the temperatures are also calibrated [36]. For each simulation, $w = 7$ parallel chains are used, with temperatures between 1 and 50 evenly spread in log space. Every 100 iterations, for each pair of chains $k, k + 1$ for $k = m, m + 2, \dots, w - 1$, the proportion of proposed swaps during those 100 iterations which were accepted is checked. (m alternates between 1 and 2 every 100 iterations.) If the acceptance proportion is too low (below 0.1), the difference in temperatures T_k and T_{k+1} is multiplied by a factor of 0.75 (the temperatures for chains $k + 1, \dots, w$ are shifted along), and if the acceptance proportion is too high (above 0.4), the difference in temperatures is multiplied by a factor of 1.5. This procedure is based on an optimal acceptance proportion of 20–23% [61, 36].

A.6 Extending the model fitted to single infection data to two strains

Section 3.2.1 in the main text mentioned that to predict the outcomes of sequential infection using the model fitted to single infection data, which only has one strain, the model was extended to two strains, assuming that the parameters for the two strains were the same. The issue arises as to how to treat the cross-reactivity parameters in the cellular adaptive immune response, as the single infection, multiple replicates data set contains no information about cross-reactivity.

To address this deficiency, before generating the results in Section 3.2, the model was re-fitted to the data, but with a fixed proportion of the cel-

lular adaptive immune response attributed to each T cell pool. Fixing this proportion ensured that when the model was extended to two strains, the proportion of cellular adaptive immunity which was cross-reactive in the fitted model was consistent with the ‘true’ parameters.

In detail, fixing this proportion was implemented by fixing the numbers of infected cells for half-maximal stimulation of naive CD8⁺ T cells k_{Cj1} to their ‘true’ values, which are the same as for the first strain in the sequential infection data. Then when we extend the model to two strains, we set k_{Cjq} to these same ‘true’ values. The scaled clearance rates of infected cells by effector CD8⁺ T cells $\bar{\kappa}_{Ejq}$ were then obtained by taking the fitted value of $\bar{\kappa}_{E11}$, and applying the formula $\bar{\kappa}_{Ejq} = \bar{\kappa}_{E11}k_{C11}/k_{Cjq}$.

B Additional results

B.1 Generated synthetic data

Figure B.1 shows the generated data for the single infection data set, while Fig. B.2 shows the generated data for the sequential infection data set, for different inter-exposure intervals. (The generated data for the sequential infection data set for the control case of a single infection is shown in Fig. 2a of the main text.)

The figures also illustrate that the model fitted to either data set accurately recovers the viral load for that data set.

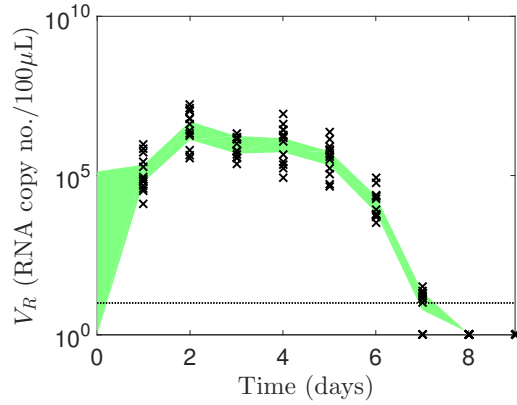


Figure B.1: *The generated single infection data.* The crosses indicate the noisy data for the thirteen ferrets. The shaded areas shows the 95% prediction interval for the viral load in the absence of noise.

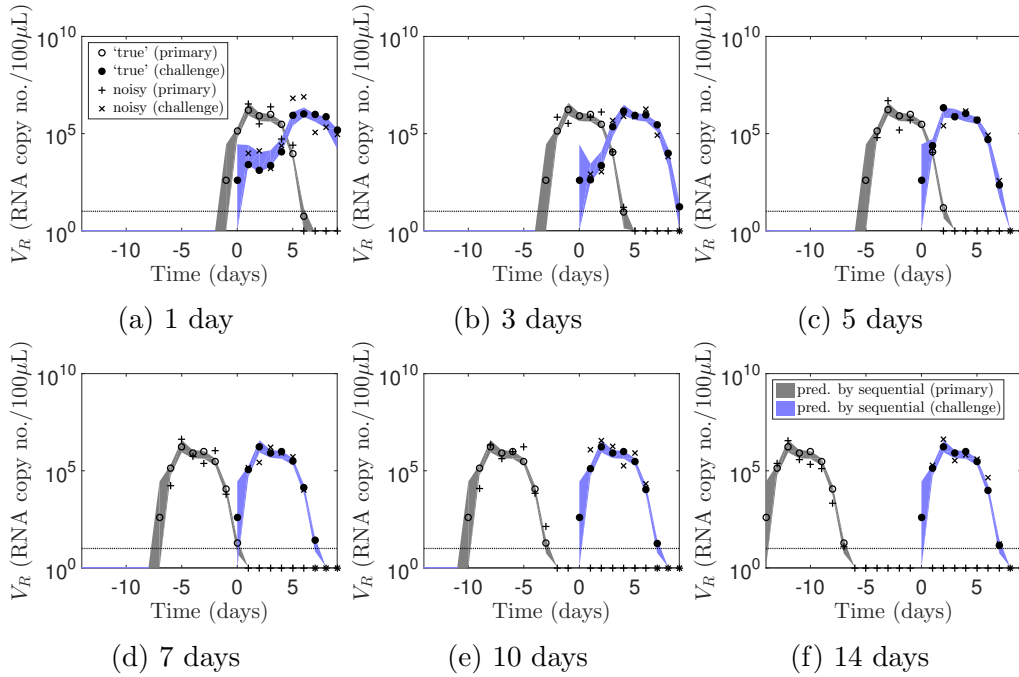


Figure B.2: *The generated sequential infection data.* The dots indicate the true viral load in the absence of noise, while the crosses indicate the noisy data. The shaded areas show 95% prediction intervals for the viral load for different inter-exposure intervals in the absence of noise.

B.2 Convergence testing

This section checks for convergence of the MCMC chains and calculates their effective sample size, as detailed in Section A.5.

Figure B.3 shows the log likelihood trace plots for the single infection and sequential infection data sets. The left-hand column shows the first 100 iterations during the calibration period; the likelihood of the random parameter values at the start of the chain is much lower than that of the values used to generate the synthetic data (horizontal line), but the likelihood quickly increases with the number of iterations. The right-hand column shows the iterations after burn-in; the log likelihood fluctuates about the likelihood for the parameters used to generate the synthetic data. This suggests that convergence has occurred.

Figures B.3a–b show trace plots for the log likelihood of an MCMC chain starting at a random point in parameter space for the single infection data set. Fig. B.3a shows the first 100 iterations during the calibration period; the likelihood of the random parameter values at the start of the chain is much lower than that of the values used to generate the synthetic data (horizontal line), but the likelihood quickly increases with the number of iterations. Fig. B.3b shows the iterations after burn-in; the log likelihood fluctuates about its value for the parameters used to generate the synthetic data. (Because noise was added to the simulated data, we do not expect the true parameters to have the maximum likelihood.) This suggests that convergence has occurred. Figures B.3c–d show similar results for the sequential infection data set.

Tables B.1 and B.2 show the potential scale reduction factor and effective sample size for each of the parameters for the single infection and sequential infection data set, after the burn-in iterations are discarded. The potential scale reduction factors are below 1.1 for every parameter, suggesting convergence; the effective sample size for each parameter is also large.

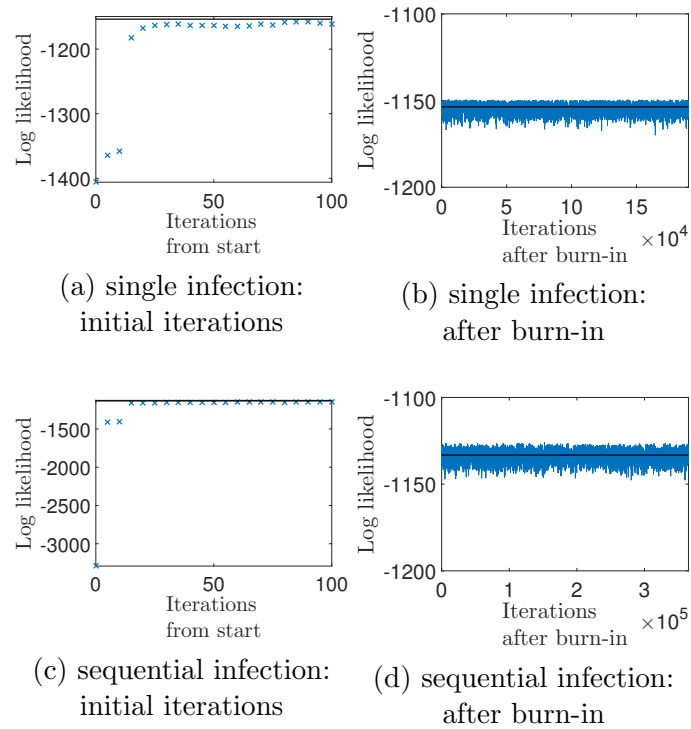


Figure B.3: Log likelihood trace plots for the fits to the single infection and sequential infection data sets. (Left) the first 100 iterations during the calibration period; (right) the iterations after burn-in. The horizontal line shows the log likelihood for the parameter values used to generate the data. The log likelihood is plotted every 5 iterations.

	Point est.	Upper C.I.	Effective sample size
$\log_{10} g$	1.00	1.00	51570.28
$\log_{10} \delta_F$	1.00	1.01	4461.84
$\log_{10} \bar{\phi}$	1.00	1.01	7721.11
$\log_{10} T_0$	1.00	1.01	18165.31
$\log_{10} \rho$	1.00	1.00	14156.31
$\log_{10} \alpha$	1.01	1.02	3290.13
$\log_{10} R_0$	1.02	1.07	1825.87
$\log_{10} r$	1.01	1.02	2102.56
$\log_{10} \delta_I$	1.01	1.03	2120.19
$\log_{10}(\delta_V - \delta_{VR})$	1.00	1.00	12768.72
$\log_{10} \delta_{VR}$	1.01	1.03	3304.28
$\log_{10} \bar{k}_F$	1.01	1.02	3441.87
$\log_{10} \bar{s}$	1.02	1.05	4609.35
$\log_{10} \bar{k}_A$	1.02	1.07	7376.80
$\log_{10} \delta_A$	1.00	1.00	112908.19
$\log_{10} \delta_B$	1.00	1.01	16218.57
$\log_{10} k_B$	1.00	1.01	26469.95
$\log_{10} \beta_B$	1.00	1.01	19694.83
$\log_{10} \tau_B$	1.01	1.03	15776.17
$\log_{10} p_R$	1.02	1.07	2488.58
$\log_{10} \gamma_0$	1.00	1.00	196077.05
$\log_{10} V_0$	1.00	1.00	6059.54
$\log_{10} \beta_C$	1.00	1.01	2880.26
$\log_{10} \delta_E$	1.01	1.03	2721.70
$\log_{10} \tau_M$	1.00	1.00	80758.58
$\log_{10} \tau_E$	1.01	1.02	2439.96
$\log_{10} \epsilon$	1.00	1.00	59634.66
$\log_{10} k_{C11}$	1.01	1.03	2967.73
$\log_{10} k_{C12}$	1.00	1.00	4373.99
$\log_{10} \bar{k}_{E11}$	1.01	1.03	2147.61
σ	1.00	1.00	92620.87

Table B.1: Potential scale reduction factor (point estimate and upper bound of 95% confidence interval) and effective sample size for each parameter, for the model fitted to the single infection data set. The first 111,000 iterations of each chain are discarded, leaving 290,001 samples from each chain and 570,003 samples across the three chains.

	Point est.	Upper C.I.	Effective sample size
$\log_{10} g$	1.00	1.00	28609.24
$\log_{10} \delta_F$	1.00	1.01	3223.48
$\log_{10} \bar{\phi}$	1.00	1.01	9489.14
$\log_{10} T_0$	1.00	1.00	39185.98
$\log_{10} \rho$	1.00	1.00	25699.60
$\log_{10} \alpha$	1.01	1.02	1478.19
$\log_{10} R_0$	1.01	1.02	1475.90
$\log_{10} r$	1.01	1.01	2347.94
$\log_{10} \delta_I$	1.01	1.01	1439.54
$\log_{10}(\delta_V - \delta_{VR})$	1.01	1.05	6465.66
$\log_{10} \delta_{VR}$	1.03	1.07	1969.53
$\log_{10} \bar{k}_F$	1.00	1.01	4532.63
$\log_{10} \bar{s}$	1.00	1.00	2527.72
$\log_{10} \bar{k}_A$	1.01	1.02	2285.39
$\log_{10} \delta_A$	1.00	1.00	95220.75
$\log_{10} \delta_B$	1.01	1.03	3047.21
$\log_{10} k_B$	1.01	1.03	3964.78
$\log_{10} \beta_B$	1.01	1.03	3503.46
$\log_{10} \tau_B$	1.03	1.10	3762.41
$\log_{10} p_R$	1.03	1.06	1229.04
$\log_{10} \gamma_0$	1.00	1.00	164376.88
$\log_{10} V_0$	1.02	1.06	1636.96
$\log_{10} \beta_C$	1.01	1.02	6123.05
$\log_{10} \delta_E$	1.01	1.03	5036.48
$\log_{10} \tau_M$	1.00	1.00	170820.42
$\log_{10} \tau_E$	1.01	1.02	4979.02
$\log_{10} \epsilon$	1.00	1.00	161894.61
$\log_{10} k_{C11}$	1.01	1.03	9151.38
$\log_{10} k_{C12}$	1.01	1.04	14663.48
$\log_{10} \bar{k}_{E11}$	1.03	1.08	2291.62
σ	1.00	1.00	44387.40

Table B.2: Potential scale reduction factor (point estimate and upper bound of 95% confidence interval) and effective sample size for each parameter, for the model fitted to the sequential infection data set. The first 35,000 iterations of each chain are discarded, leaving 165,001 samples from each chain and 495,003 samples across the three chains.

B.3 Marginal posterior distributions

This section shows histograms of samples from the marginal posterior distributions of each parameter. We emphasise that the aim of the study is not to estimate model parameters, but to quantify the roles of each immune component in controlling infection. Nonetheless, the marginal posterior distributions provide a way to gauge the additional information provided by sequential infection experiments over single infection experiments.

Furthermore, if the parameter values used to generate the synthetic data can be re-estimated, then fitting the model to real experimental data will reveal information about the rates at which processes occur in the system, which may be useful when determining reasonable parameter values for future models. On the other hand, if the marginal posterior distributions do not reflect the true parameter values, this cautions against relying on them for accurate parameter estimates.

Because of the large number of parameters, particular parameters are selected as examples of qualitative behaviours observed; the full set of marginal posterior distributions is presented in Figs. B.8–B.11 later in this section.

Some parameters are estimated accurately by the fitted models. Figure B.4 shows two examples of these parameters: the initial viral load growth rate r and the total viral decay rate δ_{VR} . To assess whether the data are informative, the marginal posterior distributions are compared to the prior distributions (leftmost column). The prior distributions are obtained by sampling from the joint prior distribution using the Metropolis algorithm as outlined in Section A.5, but setting $P(\mathbf{y}|\boldsymbol{\theta})$ to a constant.

The remaining columns show the marginal posterior distributions of the same parameter for the model fitted to the single infection and sequential infection data sets. The parameter values used to generate the data sets are marked by the vertical line.

The marginal posterior distributions indicate that the value of r can be estimated from each of the data sets, which is perhaps unsurprising because r is the initial slope of the viral load trajectory. However, the model fitted to the sequential infection data (Fig. B.4c) estimates r much more precisely. In particular, the model fitted to single infection data only (Fig. B.4b) cannot exclude the possibility that r is orders of magnitude larger than its true value. For the predicted viral load trajectory to fit the data given these large values of r , its growth rate must slow down very early on due to target cell depletion or innate immunity. The model fitted to sequential infection data is able to exclude this possibility.

Similarly, the value of the total viral load decay rate, δ_{VR} , is estimated accurately from the data. The accurate recovery of this parameter value is

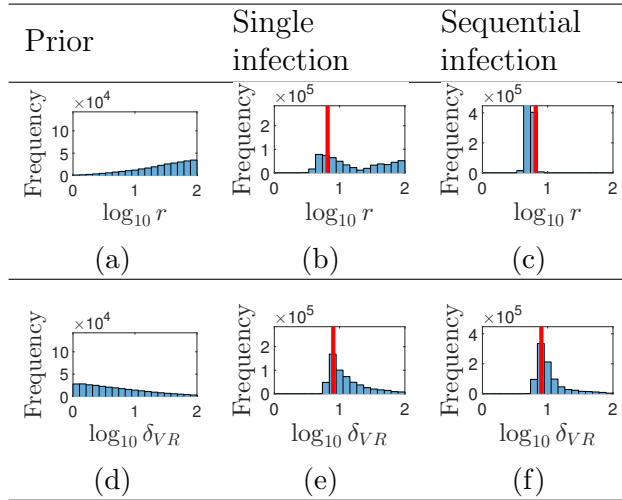


Figure B.4: *Some parameters are recovered accurately by fitting to sequential infection data.* Leftmost column: the marginal prior distribution of the parameter in the horizontal axis label. Remaining columns: the marginal posterior distributions of the same parameter for the model fitted to the data set indicated. The parameter value used to generate the data is marked by the vertical line.

because in the absence of infected cells and infectious virions, the total viral load decays at rate δ_{VR} , so the steepest negative gradient of the viral load curve during the resolution phase (on a log scale) provides a lower bound for δ_{VR} .

At the other end of the spectrum, Figs. B.5a–c show that the marginal posterior distributions for the antibody decay rate, δ_A , are the same as the marginal prior distribution. This non-identifiability occurs because the continued growth of antibodies after the end of a primary infection does not impact its viral load, and also does not impact a second infection due to the lack of cross-reactivity in the antibody response.

However, even if the marginal posterior distribution remains unchanged from the prior distribution, such that a parameter is not practically identifiable by itself, the data could contain information about a combination of parameters. Figures B.5d–f show that the marginal posterior distributions for the B cell decay rate, δ_B , are also the same as the prior distribution. However, when the value of δ_B is changed while holding all other parameters constant, the likelihood changes drastically (Fig. B.6b), whereas there is no such change for δ_A (Fig. B.6a). Hence, one cannot determine the identifiability of a parameter in combination with others by examining the marginal posterior distributions alone.

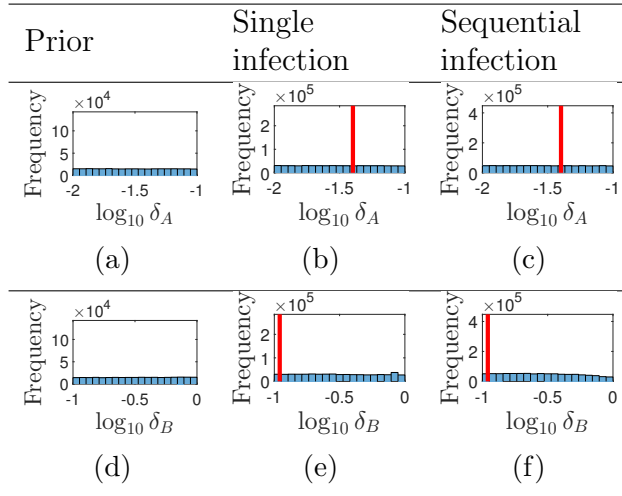


Figure B.5: *Some parameters are poorly estimated by fitting to sequential infection data.* Figure descriptions are as per Fig. B.4.

To better quantify the practical identifiability of each parameter, one could use the profile likelihood method [62]. For each parameter, as the value of the parameter is changed, the likelihood over all remaining parameters would be maximised. The maximised likelihood would only change if the target parameter can be identified from the data independently from all others. However, maximising over the large number of parameters in this model is extremely computationally costly.

Despite the lack of information in the marginal posterior distribution of some parameters (Fig. B.5 as well as many parameters in Figs. B.8–B.11), the model can fit the viral load data well, as shown in the main text. As the estimation of parameter values is not our ultimate goal, rather than relying on the marginal posterior distributions only, we use prediction methods in the main text to directly investigate how each model quantitatively attributes control of an infection to each immune component.

Further reason to use prediction methods, rather than only the marginal posterior distributions, is the apparent bias in the marginal posterior distributions for some parameters. Figure B.7 shows that the marginal posterior distributions for the basic reproduction number R_0 are biased towards much lower values than the value used to construct the synthetic data sets.

The discrepancy between the value of R_0 used to generate the synthetic data and the estimated values is of interest because previous studies have shown that R_0 for the TIV model can be written as a function of the initial viral growth rate r , the infectious cell decay rate δ_I and the infectious virion decay rate δ_V [53] — each of which are estimated in an unbiased manner

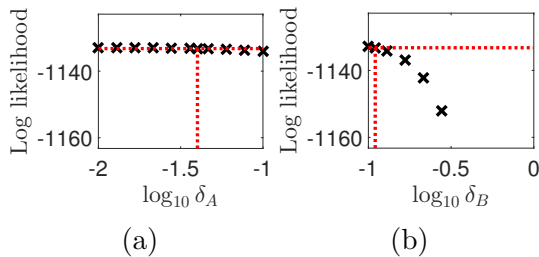


Figure B.6: *The log likelihood remains roughly constant as the value of δ_A is changed in isolation, but changes drastically when δ_B is changed.* The log likelihood for the sequential infection data set given the model parameters as (a) δ_A and (b) δ_B are varied while the other parameters are kept at the values used to generate the synthetic data. The vertical line indicates the true parameter value, and the horizontal line indicates the log likelihood of the data given the true set of parameter values.

(Fig. B.8). Moreover, in the population-scale equivalent of the TIV model — the SIR model — R_0 can be inferred reliably from data [31].

We hypothesise that contrary to initial beliefs, the estimated value of R_0 has a lesser effect in an immune-driven model than in either the TIV model, where clearance is driven by target cell depletion, or the SIR model, where similarly, the epidemic ends through depletion of susceptibles. This difference between the effects of R_0 in different models arises because in the models where resolution is driven by depletion of susceptibles (cells/individuals), the decay rate towards the end of the infection curve is either the removal rate of infectious individuals (SIR model) or a function of the non-specific decay rates of virions and infected cells (δ_I and δ_V in the TIV model). These quantities appear in R_0 . On the other hand, if resolution is driven by the immune response, the decay rate at the end of the infection is a combination of adaptive immune parameters and non-specific decay of infected cells and virions, the former of which do not appear in R_0 . Hence, although the underlying reason for the bias in the marginal posterior distribution of R_0 remains to be investigated, this parameter has less influence on the viral load than may be expected, and the viral load is nonetheless recovered accurately. This example again highlights the caution required when interpreting marginal posterior distributions.

Figures B.8–B.11 show the posterior distributions for the full set of parameters.

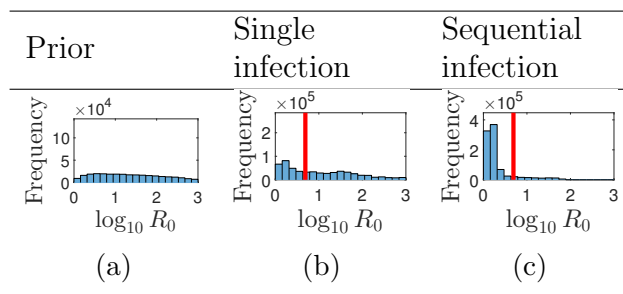


Figure B.7: *The marginal posterior distributions for R_0 are biased towards low values.* Figure descriptions are as per Fig. B.4.

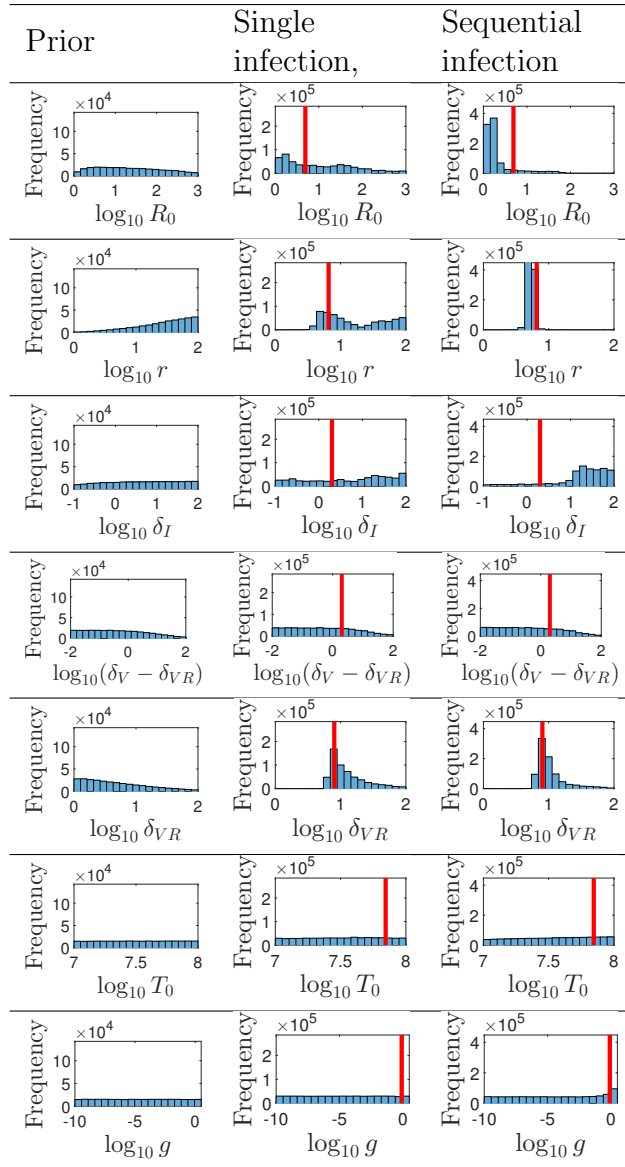


Figure B.8: The full set of marginal posterior distributions. Figure descriptions are as per Fig. B.4.

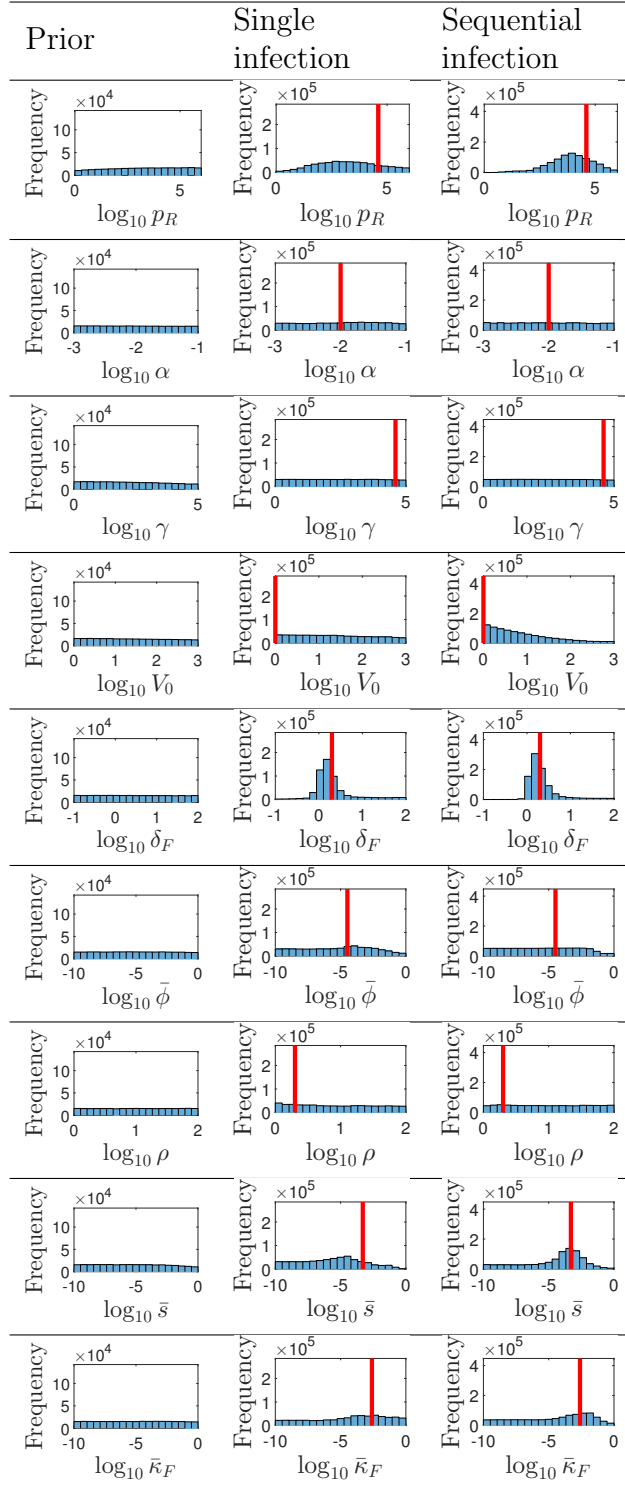


Figure B.9: Marginal distributions (continued from Fig. B.8).

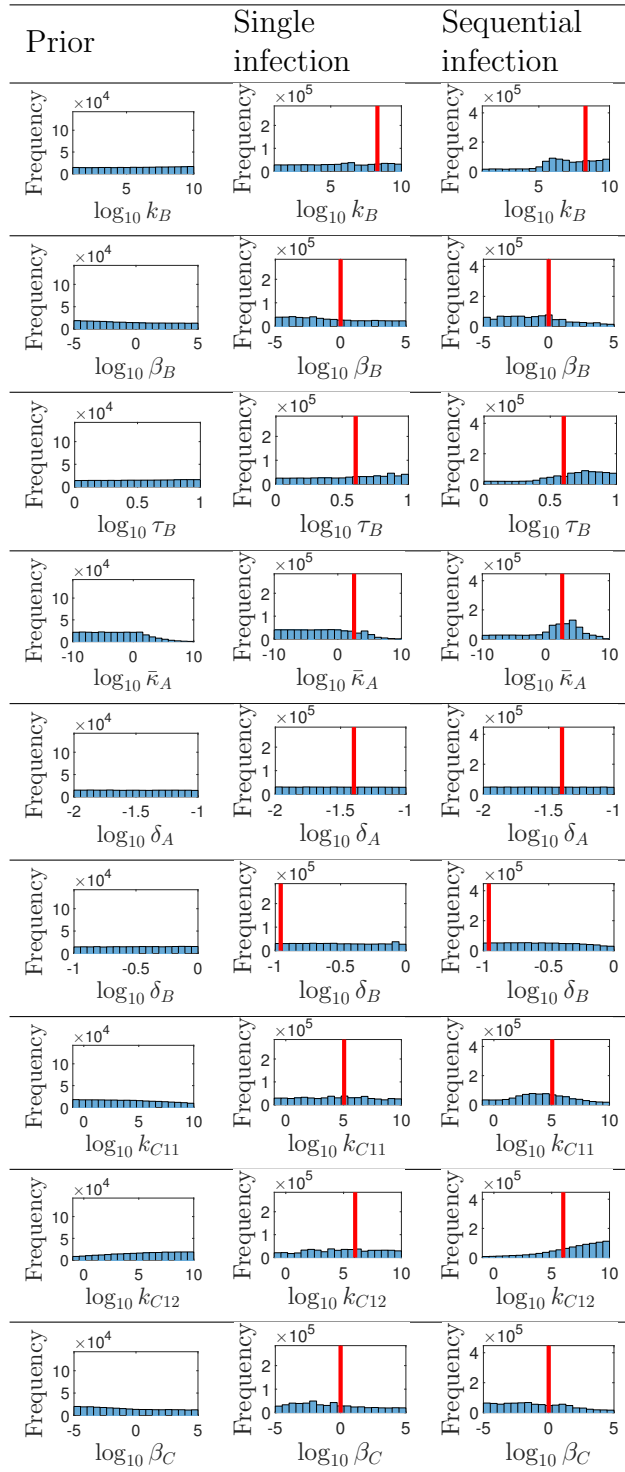


Figure B.10: Marginal distributions (continued from Fig. B.8).

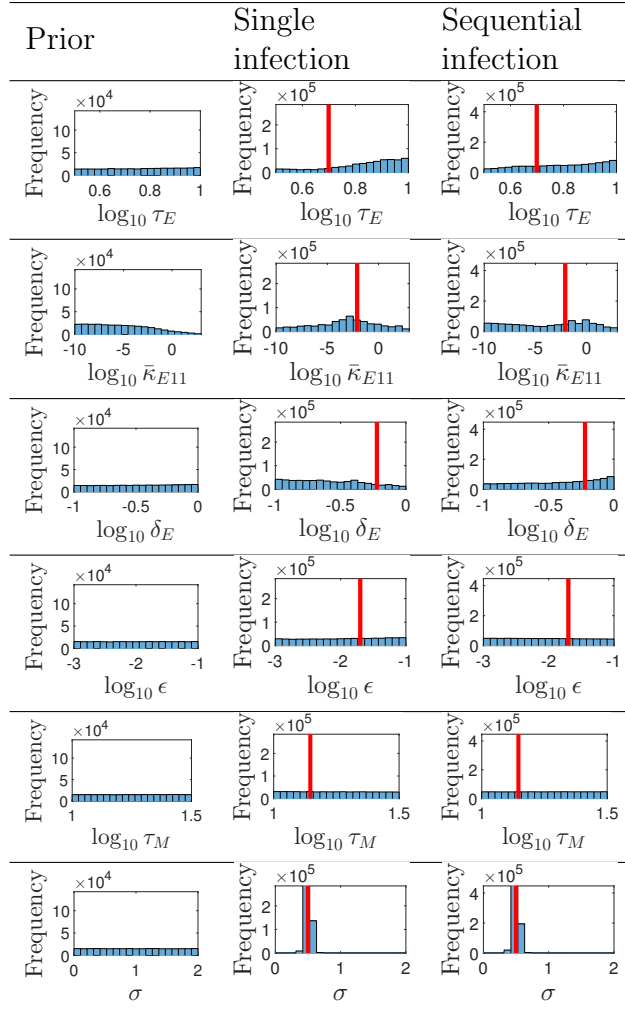


Figure B.11: Marginal distributions (continued from Fig. B.8).

B.4 Distinguishing between target cell depletion and innate immunity

Section 3.2.2 in the main text demonstrated that a model fitted to sequential infection data can distinguish whether cross-protection observed for a given inter-exposure interval is due to cellular adaptive immunity, or due to target cell depletion and/or innate immunity. This section shows that the contributions to cross-protection by target cell depletion and innate immunity cannot be reliably disentangled.

To do so, we construct a model where only innate immunity mediates cross-protection — the target cell pool is not shared between strains, and the cellular adaptive immune response is not cross-reactive (model XI, Fig. B.12). If the fitted model accurately recovers the viral load for model XI (in addition to model XIT), then it can distinguish between the contributions by target cell depletion and innate immunity to cross-protection in the synthetic data.

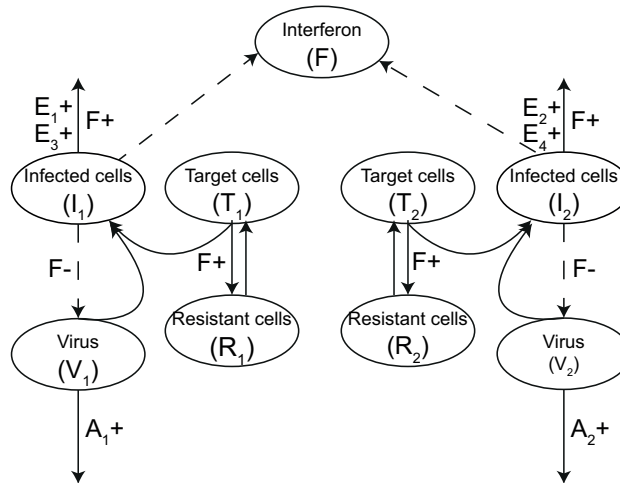


Figure B.12: A model where the two strains generate innate immune responses which are not cross-reactive (model XI).

The equations for model XI which are altered relative to Eq. A.1 are

$$\frac{dT_q}{dt} = g(T_q + R_q) \left(1 - \frac{T_q + R_q + I_q}{T_0} \right) - \beta_q T_q V_q - \bar{\phi}_q \bar{F} T_q + \rho_q R_q, \quad q = 1, \dots, Q, \quad (\text{B.1a})$$

$$\frac{dI_q}{dt} = \beta_q V_q T_q - \left(\delta_{I_q} + \bar{\kappa}_{Fq} \bar{F} + \sum_{j=1}^J \bar{\kappa}_{Ejq} \bar{E}_j \right) I_q, \quad (\text{B.1b})$$

$$\frac{dV_q}{dt} = \frac{p_{Vq}}{1 + \bar{s}_q \bar{F}} I_q - [\delta_{Vq} + \bar{\kappa}_{Aq} \bar{A}_q + \beta_q T_q] V_q, \quad (\text{B.1c})$$

$$\frac{dV_{Rq}}{dt} = \frac{p_{Vq} p_{Rq} \alpha_q}{(1 + \bar{s}_q \bar{F})} I_q - \delta_{V_{Rq}} V_{Rq} - \alpha_q \beta_q T_q V_q, \quad (\text{B.1d})$$

$$\frac{dR_q}{dt} = \bar{\phi}_q \bar{F} T_q - \rho_q R_q. \quad (\text{B.1e})$$

In addition, the same alterations to cellular adaptive immunity as model XIT are applied to model XI (the number of T cell pools in model XI is $J = 4$).

Figure B.13a shows the viral load for model XI (Fig. B.12 and Eq. B.1) generated using the ‘true’ parameters (markers) for a one-day inter-exposure interval. The delay seen in the baseline model is present, indicating that it is due to innate immunity rather than infection-induced target cell depletion. The shaded areas show the 95% prediction intervals for the viral load generated using the joint posterior distribution. The 95% prediction interval for the second strain is quite broad, suggesting that the fitted model may not correctly attribute the delay to innate immunity. To investigate this further, Fig. B.13b shows trajectories generated using 100 uniformly sampled parameter sets from the MCMC chains after burn-in. The majority of the trajectories show a delay, thus correctly attributing cross-protection in the baseline model to innate immunity; however, one trajectory (darker in colour) does not demonstrate this delay, thus incorrectly attributing cross-protection to target cell depletion. (Figure B.13c shows that if the parameter set for the darker trajectory is instead used to simulate a trajectory for model XIT, the delay is recovered, confirming that target cell depletion causes the delay for this trajectory.) This inconsistency suggests that the contributions of target cell depletion and innate immunity to cross-protection cannot be consistently distinguished. Note, however, that draws from the MCMC chains which incorrectly attribute the delay to target cell depletion constitute only a small proportion of samples.

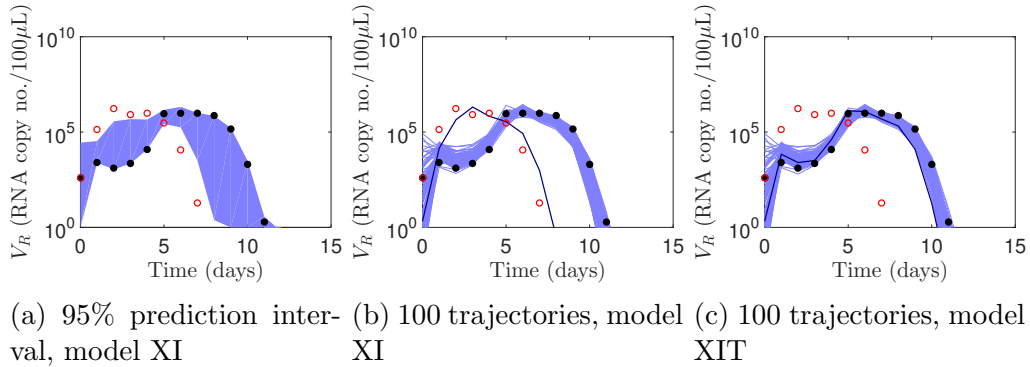


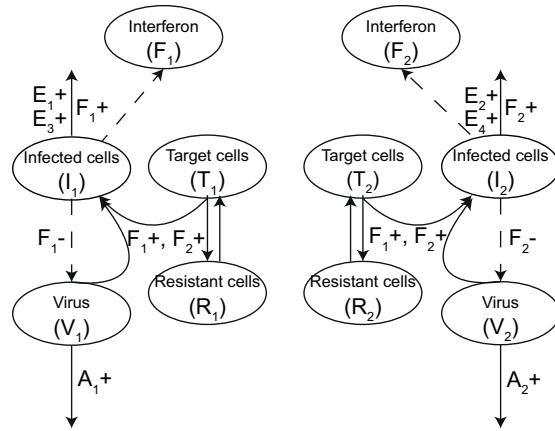
Figure B.13: *The model fitted to sequential infection data cannot consistently predict the viral load when cross-protection is mediated by innate adaptive immunity only (model XI).* (a) Comparing the challenge viral load for the ‘true’ parameter values when cross-protection is mediated by innate adaptive immunity only (model XI, black dots) to the viral load in the absence of the primary virus (red dots) shows that at a one-day inter-exposure interval, innate immunity mediates cross-protection. The model fitted to sequential infection data does not consistently predict the challenge outcome (blue, 95% prediction interval shown). (b) The markers are the same as (a); the trajectories are generated using 100 uniformly sampled parameter sets from the MCMC chains after burn-in. The darker trajectory incorrectly attributes the delay observed in the baseline model to target cell depletion rather than innate immunity. (c) Trajectories simulated using the same parameter sets as (b), but for model XIT.

B.5 Distinguishing between mechanisms of the innate immune response

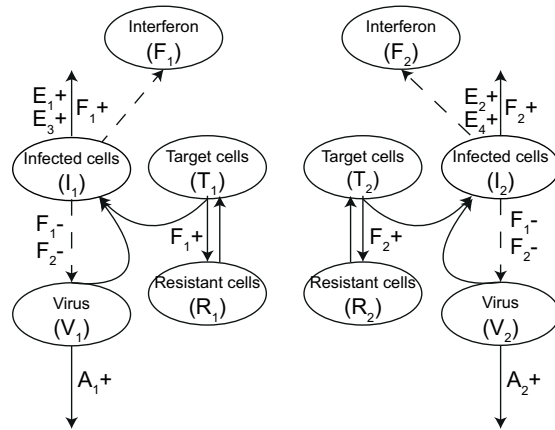
Section B.4 showed that a model fitted to sequential infection data cannot consistently distinguish between the contributions of target cell depletion and innate immunity to cross-protection. This section further demonstrates that a model fitted to sequential infection data cannot consistently determine the roles of each of the hypothesised innate immune mechanisms in controlling infection. To recap, these innate immune mechanisms are rendering target cells temporarily resistant to infection (mechanism 1); decreasing the rate at which infected cells produce virions (mechanism 2); and increasing the clearance rate of infected cells (mechanism 3).

We define the models XII–XIII (Fig. B.14) such that in each model, cells infected with strain q induce the production of interferon specific to strain q . In model XII y , cross-protection is only mediated by innate immune mech-

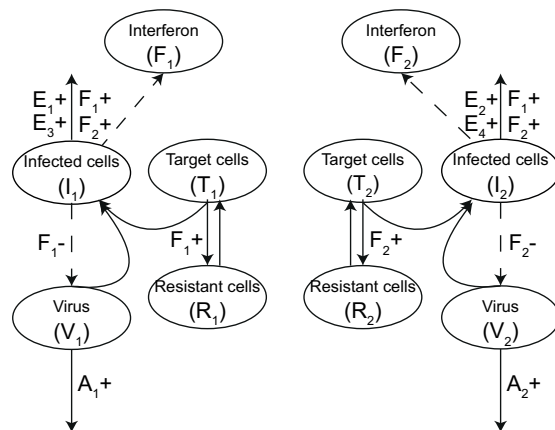
anism y , and not by the other innate immune mechanisms, target cell depletion, or cellular adaptive immunity.



(a) Model XI1: cross-protection mediated by interferon rendering target cells temporarily resistant to infection



(b) Model XI2: cross-protection mediated by interferon decreasing the production rate of virions from infected cells



(c) Model XI3: cross-protection mediated by interferon increasing the clearance rate of infected cells

Figure B.14: Three alternative models, where in model XI y , cross-protection is only mediated by innate immune mechanism y , and not by the other innate immune mechanisms, target cell depletion, or cellular adaptive immunity.

Equations B.2–B.4 show the equations which are changed in models XI1–XI3 relative to the baseline model (Eq. A.1).

$$\frac{dT_q}{dt} = g(T_q + R_q) \left(1 - \frac{T_q + R_q + I_q}{T_0} \right) - \beta_q T_q V_q - \bar{\phi}_q \left(\sum_{q'=1}^Q \bar{F}_{q'} \right) T_q + \rho_q R_q, \quad (\text{B.2a})$$

$$\frac{dI_q}{dt} = \beta_q V_q T_q - \left(\delta_{I_q} + \bar{\kappa}_{Fq} \bar{F}_q + \sum_{j=1}^J \bar{\kappa}_{Ejq} \bar{E}_j \right) I_q, \quad (\text{B.2b})$$

$$\frac{dV_q}{dt} = \frac{pV_q}{1 + \bar{s}_q \bar{F}_q} I_q - [\delta_{V_q} + \bar{\kappa}_{Aq} \bar{A}_q + \beta_q T_q] V_q, \quad (\text{B.2c})$$

$$\frac{dV_{Rq}}{dt} = \frac{pV_q p_{Rq} \alpha_q}{1 + \bar{s}_q \bar{F}_q} I_q - \delta_{V_{Rq}} V_{Rq} - \alpha_q \beta_q T_q V_q, \quad q = 1, \dots, Q, \quad (\text{B.2d})$$

$$\frac{dR_q}{dt} = \bar{\phi}_q \left(\sum_{q'=1}^Q \bar{F}_{q'} \right) T_q - \rho_q R_q, \quad (\text{B.2e})$$

$$\frac{d\bar{F}_q}{dt} = \bar{p}_{Fq} I_q - \delta_{Fq} \bar{F}_q. \quad (\text{B.2f})$$

$$\frac{dT_q}{dt} = g(T_q + R_q) \left(1 - \frac{T_q + R_q + I_q}{T_0} \right) - \beta_q T_q V_q - \bar{\phi}_q \bar{F}_q T_q + \rho_q R_q, \quad (\text{B.3a})$$

$$\frac{dI_q}{dt} = \beta_q V_q T_q - \left(\delta_{I_q} + \bar{\kappa}_{Fq} \bar{F}_q + \sum_{j=1}^J \bar{\kappa}_{Ejq} \bar{E}_j \right) I_q, \quad (\text{B.3b})$$

$$\frac{dV_q}{dt} = \frac{pV_q}{1 + \bar{s}_q \left(\sum_{q'=1}^Q \bar{F}_{q'} \right)} I_q - [\delta_{V_q} + \bar{\kappa}_{Aq} \bar{A}_q + \beta_q T_q] V_q, \quad (\text{B.3c})$$

$$\frac{dV_{Rq}}{dt} = \frac{pV_q p_{Rq} \alpha_q}{1 + \bar{s}_q \left(\sum_{q'=1}^Q \bar{F}_{q'} \right)} I_q - \delta_{V_{Rq}} V_{Rq} - \alpha_q \beta_q T_q V_q, \quad q = 1, \dots, Q, \quad (\text{B.3d})$$

$$\frac{dR_q}{dt} = \bar{\phi}_q \bar{F}_q T_q - \rho_q R_q, \quad (\text{B.3e})$$

$$\frac{d\bar{F}_q}{dt} = \bar{p}_{Fq} I_q - \delta_{Fq} \bar{F}_q. \quad (\text{B.3f})$$

$$\frac{dT_q}{dt} = g(T_q + R_q) \left(1 - \frac{T_q + R_q + I_q}{T_0}\right) - \beta_q T_q V_q - \bar{\phi}_q \bar{F}_q T_q + \rho_q R_q, \quad (\text{B.4a})$$

$$\frac{dI_q}{dt} = \beta_q V_q T_q - \left[\delta_{I_q} + \bar{\kappa}_{Fq} \left(\sum_{q'=1}^Q \bar{F}_{q'} \right) + \sum_{j=1}^J \bar{\kappa}_{Ejq} \bar{E}_j \right] I_q, \quad (\text{B.4b})$$

$$\frac{dV_q}{dt} = \frac{p_{Vq}}{1 + \bar{s}_q \bar{F}_q} I_q - [\delta_{Vq} + \bar{\kappa}_{Aq} \bar{A}_q + \beta_q T_q] V_q, \quad (\text{B.4c})$$

$$\frac{dV_{Rq}}{dt} = \frac{p_{Vq} p_{Rq} \alpha_q}{1 + \bar{s}_q \bar{F}_q} I_q - \delta_{V_{Rq}} V_{Rq} - \alpha_q \beta_q T_q V_q, \quad q = 1, \dots, Q, \quad (\text{B.4d})$$

$$\frac{dR_q}{dt} = \bar{\phi}_q \bar{F}_q T_q - \rho_q R_q, \quad (\text{B.4e})$$

$$\frac{d\bar{F}_q}{dt} = \bar{p}_{Fq} I_q - \delta_{Fq} \bar{F}_q. \quad (\text{B.4f})$$

Figure B.15 shows the viral load predicted by the ‘true’ parameters for each of models XI1–XI3 (black dots), for the sequential infection data set and a one-day inter-exposure interval. Comparing these to the viral load in the absence of the primary virus (red dots) shows that the delay in the baseline model occurs due to a combination of innate immune mechanisms 2 and 3. The trajectories in Fig. B.15 are simulated using 100 uniformly sampled parameter sets from the MCMC chains after burn-in (the same parameter sets as Fig. B.13). The discrepancy between the trajectories and the black dots indicates that the fitted model cannot attribute cross-immunity to the correct mechanisms of the innate immune response. In particular, some trajectories simulated using each of models XI1–XI3 show a marked delay in the second infection, incorrectly attributing the delay in the baseline model fully to a single innate immune mechanism.

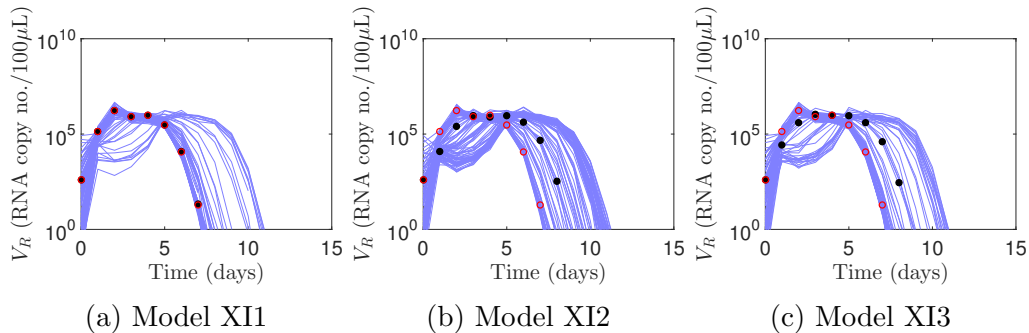


Figure B.15: *The model fitted to sequential infection data cannot predict the viral load for models where cross-protection is mediated only by one innate immune mechanism (models XI1–XI3).* The challenge viral load for the ‘true’ parameter values when cross-protection is mediated by only one innate immune mechanism (models XI1–XI3, black dots) is compared to the viral load in the absence of the primary virus (red dots). At a one-day inter-exposure interval, the delay in the baseline model occurs due to a combination of innate immune mechanisms 2 and 3. The trajectories are simulated using 100 uniformly sampled parameter sets from the MCMC chains after burn-in (the same parameter sets as Fig. B.13). The discrepancy between the trajectories and the markers indicates that the fitted model cannot attribute cross-immunity to the correct mechanisms of the innate immune response.

B.6 Estimating the initial growth rate of the second virus for different inter-exposure intervals

Sections 3.2.1 and 3.2.2 in the main text showed that a model fitted to sequential infection data captures the timing and strength of cross-protection between strains, and correctly distinguishes the contributions of cellular adaptive immunity and target cell depletion/innate immunity to this cross-protection. We will now demonstrate that the model is able to do so partly through capturing the effect of a first infection on the initial growth rate of the second.

Analogous to Eq. A.1, we define the initial growth rate for the second

strain when there is a time-dependent immune response to be

$$r_2(t) = -\frac{\widehat{\delta}_{I2} + \widehat{\delta}_{V2}}{2} + \frac{\sqrt{(\widehat{\delta}_{I2} - \widehat{\delta}_{V2})^2 + 4\beta T(t)\widehat{p}_V}}{2} \quad \text{where} \quad (\text{B.5a})$$

$$\widehat{p}_V = \frac{p_V}{1 + \bar{s}\bar{F}(t)}, \quad (\text{B.5b})$$

$$\widehat{\delta}_{V2} = \beta T(t) + \delta_V + \bar{\kappa}_A \bar{A}_2(t), \quad (\text{B.5c})$$

$$\widehat{\delta}_{I2} = \delta_I + \bar{\kappa}_F \bar{F}(t) + \sum_{j=1}^J \bar{\kappa}_{Ej2} \bar{E}_j(t). \quad (\text{B.5d})$$

This equation is derived from Eq. A.1 by replacing the number of target cells, T , the production rate of virions from infected cells, p_V , the decay rate of virions, δ_V , and the decay rate of infected cells δ_I , with their time-dependent versions for the second strain when the immune response is active.

The value of $r_2(t)$ at (and shortly after) the time of exposure to the second virus dictates the initial growth of the second virus — whether it grows rapidly (as if the first virus were not present), or whether it is suppressed. Hence, it measures the timing and strength of cross-protection between strains. Accurate prediction of $r_2(t)$ across a wide timespan enables prediction of the early time course of the second virus for different inter-exposure intervals, as examined in Section 3.2.1 of the main text.

Note that by construction, the trajectories for $T(t)$, $\bar{F}(t)$, $\bar{E}_j(t)$ and $\bar{A}_2(t)$ are assumed to be changing due to the first virus only, which is approximately true during early infection. (Hence, $\bar{A}_2(t)$ is zero at all times; $T(t)$, $\bar{F}(t)$ and $\bar{E}_j(t)$ are the solutions to the model equations for a single infection.)

B.6.1 The timing and extent of cross-protection between strains

This section will show that a model fitted to sequential infection data accurately recovers $r_2(t)$, and thus captures the timing and strength of cross-protection. On the other hand, a model fitted to single infection data does not accurately recover $r_2(t)$.

In Fig. B.16a, the ‘true’ parameters for the sequential infection data set are used to evaluate $r_2(t)$ (markers). The ‘true’ value of $r_2(t)$ is close to zero for 2–5 days after the first exposure. This reflects suppression of the growth of the second strain if it is introduced shortly before or during this period. Conversely, the high value of $r_2(t)$ before and after this period suggests that for shorter or longer inter-exposure intervals, the viral load of the second strain initially grows exponentially.

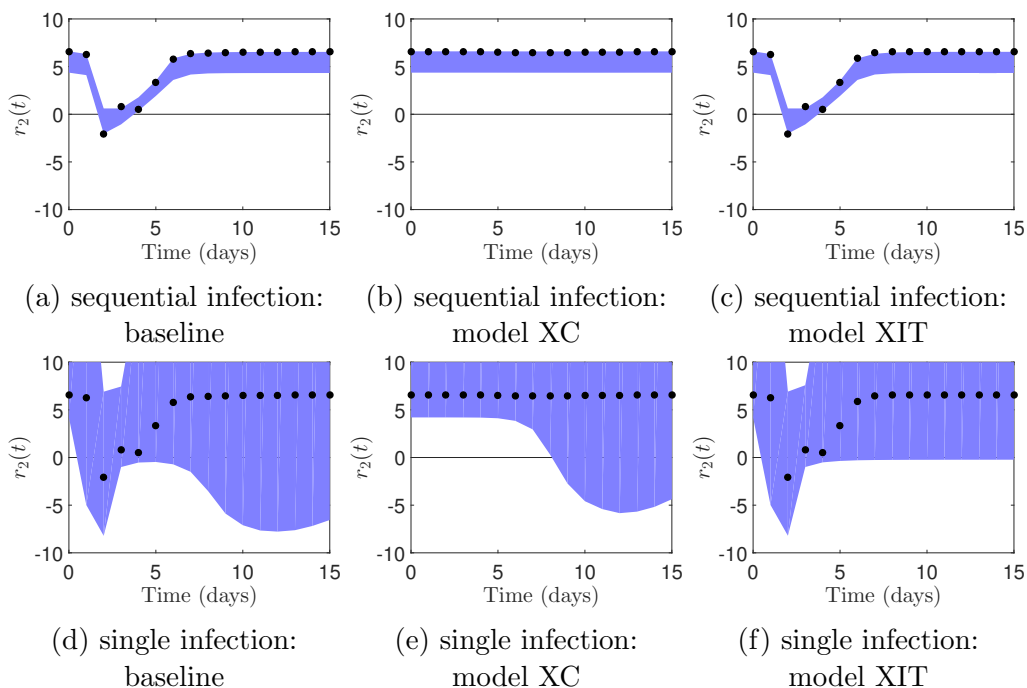


Figure B.16: *The model fitted to sequential infection data captures the initial growth rate of the second virus ($r_2(t)$), but the model fitted to single infection data does not.* Top: The ‘true’ parameters for the sequential infection data set are used to evaluate $r_2(t)$ for the second strain (markers) for (a) the baseline model; (b) model XC; (c) model XIT. Samples from the joint posterior distribution are then used to predict the same quantity (95% prediction intervals shown). The horizontal axis indicates time after the first exposure. Bottom: as per above, but for the single infection data set.

Samples from the joint posterior distribution are then used to predict the same quantity (95% prediction interval shown). The model accurately recovers $r_2(t)$, enabling it to predict the time course of early infection with the second virus for different inter-exposure intervals.

On the other hand, the model fitted to single infection data does not accurately recover $r_2(t)$ (Fig. B.16d), despite capturing a single infection viral load curve well. This suggests that the model does not attribute the features of the viral load trajectory for a single infection to the correct components of the immune response.

B.6.2 Determining the contribution of cellular adaptive immunity to cross-protection

This section will show that a model fitted to sequential infection data accurately predicts how $r_2(t)$ changes when the baseline model is modified. The first modification is such that cross-protection is only mediated by cellular adaptive immunity, but not target cell depletion or innate immunity (model XC); the second modification is such that cross-protection is only mediated by target cell depletion and innate immunity, but not cellular adaptive immunity (model XIT). As a result, the model recovers the degree to which cross-protection in the ‘true’ model is due to either cellular adaptive immunity, or target cell depletion/innate immunity. On the other hand, the model fitted to single infection data poorly captures the contribution of these components to cross-protection.

For model XC, the expression for $r_2(t)$ is obtained by substituting $\bar{F}(t) \rightarrow 0$ and $T(t) \rightarrow T_0$ in Eq. B.5. For model XIT, the expression for $r_2(t)$ is obtained by substituting $\bar{E}_j(t) \rightarrow 0$.

First, for the sequential infection data set, we analyse how $r_2(t)$ changes for the ‘true’ parameter values in models XC and XIT (markers in Fig. B.16b–c) compared to the baseline model (markers in Fig. B.16a). When cross-reactivity is mediated by cellular adaptive immunity only (model XC), $r_2(t)$ is roughly constant; by contrast, when cross-reactivity is mediated by target cell depletion and innate immunity only (model XIT), $r_2(t)$ is close to that for the baseline model. These changes to $r_2(t)$ confirm that for the ‘true’ parameters, the baseline model attributes little cross-protection to cellular adaptive immunity.

Figures B.16b–c show that the model fitted to the sequential infection data set accurately recovers $r_2(t)$ for models XC and XIT. This enables it to capture the low contribution of cellular adaptive immunity to cross-protection.

On the other hand, the joint posterior distribution from the model fitted to the single infection data set does not accurately recover $r_2(t)$ for models XC and XIT (Figs. B.16e–f). Figure B.16e shows that the fitted model captures $r_2(t)$ for model XC (where cross-protection is mediated by cellular adaptive immunity only) for short inter-exposure intervals, but not long inter-exposure intervals. This result is consistent with the finding in Section 3.2.2 of the main text that the model fitted to the single infection data correctly infers that cellular adaptive immunity has little effect shortly after the first exposure, but does not capture its longer term effects. By contrast, Fig. B.16f shows that the combined effects of target cell depletion and innate immunity on the early growth of the second virus are not captured by the model fitted

to the single infection data at any time.

B.7 Determining the timing and role of humoral and cellular adaptive immunity in controlling a single infection

Given that a model fitted to sequential infection data accurately recovers the viral load when the adaptive immune response is removed (Section 3.2.3 in the main text), it is natural to ask whether such a model would still recover the viral load accurately if only the humoral adaptive immune response or only the cellular adaptive immune response were removed. Figure B.17 shows that a model fit to sequential infection data cannot predict how the viral load for the decay phase changes when (a) the humoral adaptive immune response or (b) the cellular adaptive immune response is removed. This implies that it cannot distinguish the contributions of antibodies and cellular adaptive immunity to resolution of the infection.

In detail, the ‘true’ parameters predict that when humoral adaptive immunity is disabled, the viral load rebounds instead of continuing to decrease (black markers in Fig. B.17a). Trajectories simulated from the joint posterior distribution for the model fitted to sequential infection data cannot consistently recover this result. Some trajectories predict that resolution of the infection is delayed, while others predict that the viral load stays at a constant level.

The ‘true’ parameters also predict that when cellular adaptive immunity is disabled, resolution of the infection is delayed (black markers in Fig. B.17b). The fitted model’s predictions range from no delay to a chronic infection. Hence, it does not capture the contribution of cellular adaptive immunity to resolution of the infection.

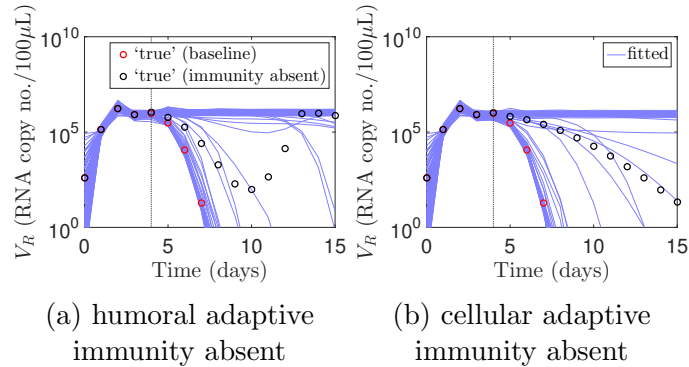


Figure B.17: *A model fitted to sequential infection data cannot predict how the viral load trajectory for the decay phase changes when the humoral adaptive immune response or the cellular adaptive immune response is removed.* The vertical lines indicate, for the ‘true’ parameter values, the times at which (a) humoral immunity and (b) cellular immunity take effect. These are determined by when the viral load for the baseline model (black dots) deviates from the viral load when (a) humoral immunity and (b) cellular immunity are absent (red dots). The model fitted to sequential infection data recovers both of these times (100 predicted trajectories for the viral load shown in blue), but cannot predict the viral load afterwards.

B.8 Predicting the trajectory of compartments other than the viral load

The main text mentions a limitation of fitting a model to sequential infection data: that the fitted model cannot predict the trajectory of compartments other than the total viral load. As this limitation is not directly linked to the immune response, it is explored in this appendix rather than the main text. Figure B.18 shows (left) the number of target cells, (centre) the number of infected cells, and (right) the infectious viral load for a single infection, for the ‘true’ parameters (markers). The shaded areas show the 95% prediction intervals generated using the joint posterior distribution from a model fitted to (top) sequential infection and (bottom) single infection data.

The model fitted to sequential infection data accurately predicts that target cells do not become depleted during the course of infection (Fig. B.18a), but the model fit to single infection data does not consistently do so (Fig. B.18d). This result indicates that the model fitted to the single infection data set may attribute resolution of the infection to target cell depletion rather than the immune response.

However, the models fitted to either data set have very wide 95% pre-

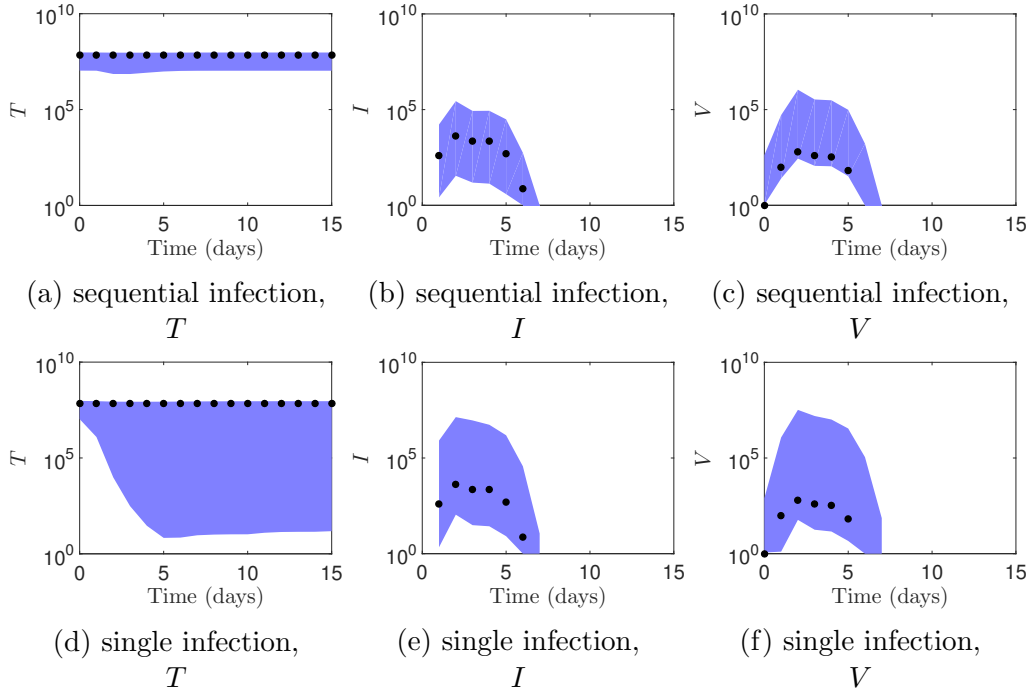


Figure B.18: *The 95% prediction intervals for the number of target cells, the number of infected cells and the number of infectious virions are wide regardless of whether the model is fitted to sequential infection or single infection data.* (a–c): The ‘true’ parameters for the sequential infection data set are used to simulate the trajectories (markers) for (a) the number of target cells, (b) the number of infected cells, and (c) the infectious viral load for a single infection. The shaded area shows the 95% prediction interval generated using the joint posterior distribution from the fitted model. (d–f): As per (a–c), but for the single infection data set.

diction intervals for the number of infected cells (Figs. B.18b and B.18e), as well as the number of infectious virions (Figs. B.18c and B.18f). This uncertainty may become an issue if one is intrinsically interested in the time course of these compartments. However, it may not affect the main aim of the study, which is to quantify the role of each immune component in controlling infection.

C Additional results for a sequential infection, high cross-reactivity data set

C.1 The sequential infection, high cross-reactivity data set

Appendix C presents results for an additional set of parameters where the degree of cross-reactivity in the cellular adaptive immune response is high. In this case, the qualitative behaviour of the model for sequential infections matches the experiments by Laurie et al. [38] when infection is with influenza A strains of different subtypes (A(H1N1)pdm09 and A(H3N2)).

- For short inter-exposure intervals (1–3 days), co-infection with both viruses is observed;
- for medium inter-exposure intervals (5–7 days), the second infection is prevented;
- for long inter-exposure intervals (10–14 days), the second infection is shortened.

The parameters for the high cross-reactivity data set are the same as for the low cross-reactivity data set, except for the cross-reactivity parameters. Instead of the parameter values given in Table A.3, $\log_{10} k_{C11} = \log_{10} k_{C22} = 6$ and $\log_{10} k_{C13} = \log_{10} k_{C23} = 5.05$.

C.2 Results

In this section, we present results for the high-cross-reactivity data set corresponding to those in Section 3 of the main text.

C.2.1 Goodness of fit of the model to the generated synthetic data

First, we establish that the model recovers the viral load when fitted to the sequential infection, high cross-reactivity data. Figure C.1a presents prediction intervals for the viral load for a single infection. The prediction intervals include the ‘true’ viral load, confirming the goodness of fit of the model when fitted to either data set.

Figures C.1b and C.1c show the viral load for different inter-exposure intervals, predicted by the model fitted to the high cross-reactivity data. The grey and blue areas, which show the 95% prediction intervals for the

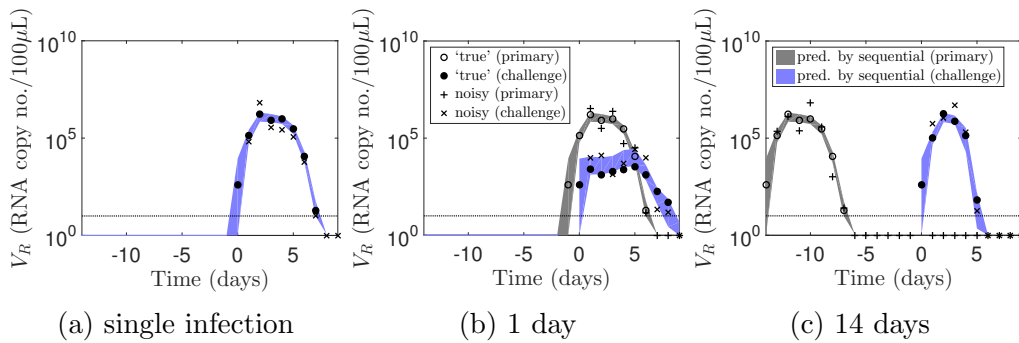


Figure C.1: *The generated data and prediction intervals for the viral load, for the model fitted to the sequential infection, high cross-reactivity data set. The prediction intervals include the ‘true’ viral load, confirming the goodness of fit of the model. (a) The dots show the viral load for a single infection simulated using the model and the ‘true’ parameters. The viral load with measurement noise is shown as crosses. The shaded area is the 95% prediction interval for the viral load generated using the joint posterior distribution for the parameters, obtained by fitting the model to the sequential infection, high cross-reactivity data. (b–c) The viral load is simulated for sequential infections with the labelled inter-exposure interval. The open and closed dots show the viral load for a primary and challenge infection respectively. The grey and blue areas show the 95% prediction intervals for the primary and challenge viral load respectively.*

primary and challenge viral load respectively, demonstrate a good fit of the model to the data.

C.2.2 Recovering immunological quantities

Determining the timing and extent of cross-protection between strains

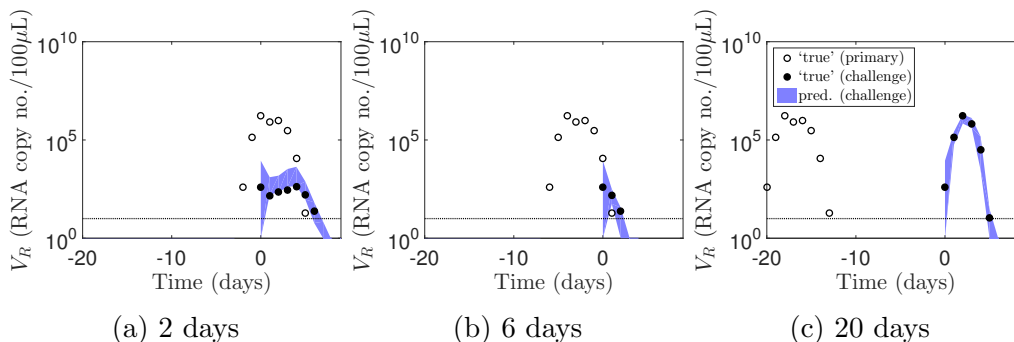


Figure C.2: A model fitted to sequential infection data can predict outcomes of further sequential infection experiments using the same strains. The dots show the viral load for inter-exposure intervals of 2, 6 and 20 days, simulated using the ‘true’ parameters (shown without measurement noise). The shaded areas show the 95% prediction intervals for the viral load of the challenge strain (without measurement noise) for these inter-exposure intervals.

Analogous to Fig. 3 in the main text, Fig. C.2 shows prediction intervals for the viral load for inter-exposure intervals of 2, 6 and 20 days, which were not included in the high cross-reactivity data. The fitted model accurately predicts the viral load for the challenge strain, including (a) co-infection with the two strains; (b) prevention of the second infection; and (c) shortening of the second infection. These results indicate that a model fitted to sequential infection, high cross-reactivity data captures the timing and extent of cross-protection.

Determining the cross-protection conferred by each immune component

Following the argument in Section 3.2.2 of the main text, first we extract the contributions to cross-protection by either cellular adaptive immunity, or target cell depletion/innate immunity, for the ‘true’ parameter values.

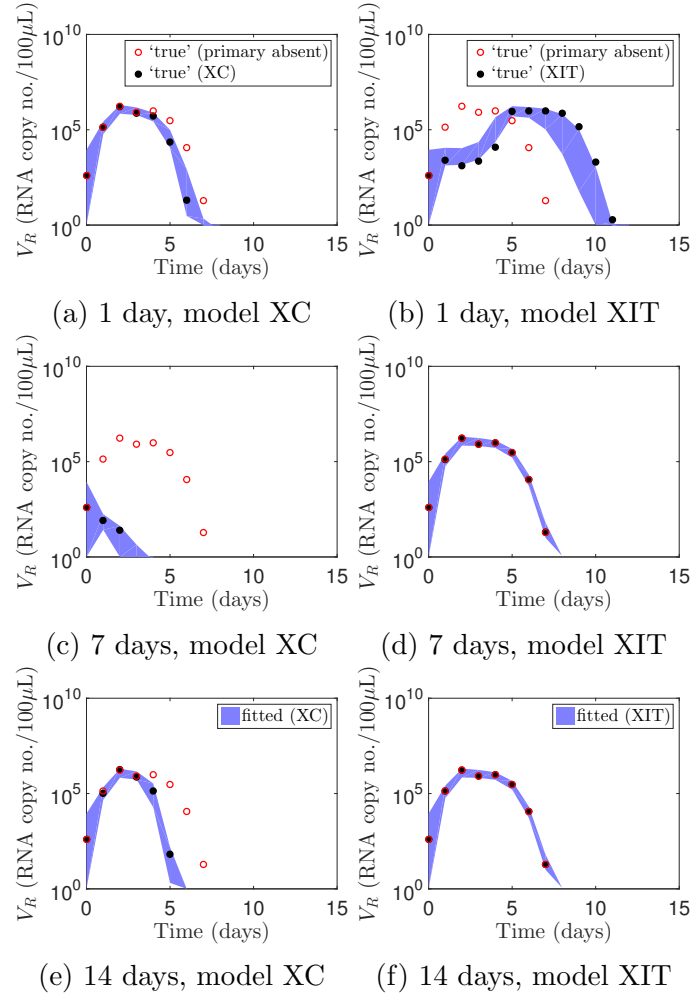


Figure C.3: A model fitted to sequential infection, high cross-reactivity data accurately predicts the challenge viral load when the mechanisms mediating cross-protection are restricted. Comparing the challenge viral load for the ‘true’ parameter values when the mechanisms mediating cross-protection are restricted (models XC and XIT, black dots) to the viral load in the absence of the primary virus (red dots) shows that at a one-day inter-exposure interval, target cell depletion and/or innate immunity delay the second infection, whereas cellular adaptive immunity is responsible for timely resolution of the infection; and at seven-day and 14-day inter-exposure intervals, cellular adaptive immunity mediates cross-protection. The model fitted to sequential infection, high cross-reactivity data accurately predicts the challenge outcomes (95% prediction intervals shaded).

Figure C.3 shows predictions of the challenge viral load using models XC and XIT for these values (black dots). (Recall that in model XC, cross-protection is mediated by cellular adaptive immunity rather than target cell depletion/innate immunity, while in model XIT, cross-protection is mediated by target cell depletion/innate immunity rather than cellular adaptive immunity.) Comparing these predictions to the viral load in the absence of the primary virus (red dots), we see that at a one-day inter-exposure interval, target cell depletion and/or innate immunity suppress infection with the second strain (Fig. C.3b). Figure C.3b also shows that resolution of the second infection is delayed if cross-protection is mediated by target cell depletion/innate immunity only. This delay is not observed for the baseline model (Fig. C.1b), suggesting that cellular adaptive immunity contributes to timely resolution of the infection. Indeed, we see in Fig. C.3a that the second infection is slightly shortened when only cellular adaptive immunity mediates cross-protection.

For seven and 14-day inter-exposure intervals, only cellular adaptive immunity mediates cross-protection (either preventing or shortening the second infection). This is evidenced by the protection observed for model XC (Fig. C.3c,e) but not model XIT (Fig. C.3d,f).

In each scenario, the model fitted to sequential infection, high cross-reactivity data accurately predicts challenge outcomes (shaded areas). This result demonstrates that the fitted model captures the cross-protection conferred by either cellular adaptive immunity, or a combination of target cell depletion and innate immunity.

Determining the timing and role of each immune component in controlling a single infection

Figure C.4 shows that the model fitted to sequential infection, high cross-reactivity data predicts features of the viral load for a single infection when various immune components are absent.

Figure C.4a shows that the model fitted to sequential infection, high cross-reactivity data accurately captures the timing of adaptive immunity by recovering the time at which the viral load when adaptive immunity is absent (black dots) deviates from the baseline model (red dots); this time is indicated by the vertical line. In addition, the fitted model predicts correctly that the infection does not resolve in the absence of adaptive immunity.

Figure C.4b shows that the model fitted to sequential infection, high cross-reactivity data recovers the time at which the viral load deviates from the baseline model when both innate and adaptive immunity are absent.

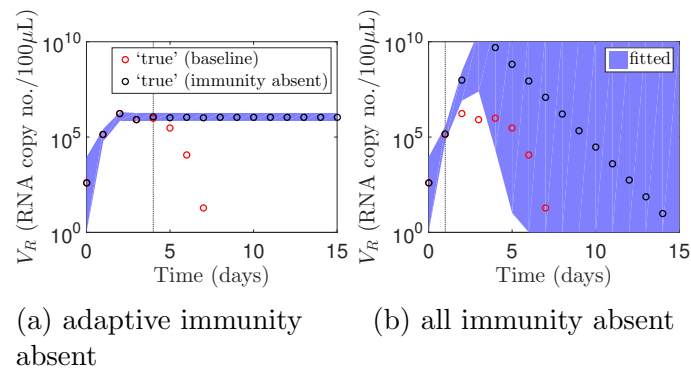


Figure C.4: *The model fitted to sequential infection, high cross-reactivity data predicts features of the viral load for a single infection when various immune components are absent.* The vertical lines indicate, for the ‘true’ parameter values, the times at which (a) adaptive immunity and (b) innate immunity take effect. These are determined by when the viral load for the baseline model (black dots) deviates from the viral load when (a) adaptive immunity and (b) both innate and adaptive immunity are absent (red dots). The model fitted to sequential infection, high cross-reactivity data recovers both of these times (95% prediction intervals for the viral load shown in blue). In addition, the fitted model accurately predicts that the infection does not resolve in the absence of adaptive immunity.

However, the fitted model does not accurately predict how the infection resolves in the absence of innate and adaptive immunity. This result is the same as that for the low cross-reactivity data set.

References

- [1] Ahmed, H., Moore, J., Manicassamy, B., Garcia-Sastre, A., Handel, A., & Antia, R. (2017). Mathematical analysis of a mouse experiment suggests little role for resource depletion in controlling influenza infection within host. *ArXiv e-prints*, .
- [2] Ahn, J. E., Karlsson, M. O., Dunne, A., & Ludden, T. M. (2008). Likelihood based approaches to handling data below the quantification limit using NONMEM VI. *J Pharmacokinet. Pharmacodyn.*, *35*, 401–421. doi:10.1007/s10928-008-9094-4.
- [3] Arenas, A. R., Thacker, N. B., & Haskell, E. C. (2017). The logistic growth model as an approximating model for viral load measurements

- of influenza A virus. *Math. Comput. Simul.*, *133*, 206–222. doi:10.1016/j.matcom.2016.10.002.
- [4] Baccam, P., Beauchemin, C., Macken, C. A., Hayden, F. G., & Perelson, A. S. (2006). Kinetics of influenza A virus infection in humans. *J. Virol.*, *80*, 7590–7599. doi:10.1128/JVI.01623-05.
- [5] Barchet, W., Oehen, S., Klenerman, P., Wodarz, D., Bocharov, G., Lloyd, A. L., Nowak, M. A., Hengartner, H., Zinkernagel, R. M., & Ehl, S. (2000). Direct quantitation of rapid elimination of viral antigen-positive lymphocytes by antiviral CD8(+) T cells in vivo. *Eur. J. Immunol.*, *30*, 1356–63. doi:10.1002/(SICI)1521-4141(200005)30:5<1356::AID-IMMU1356>3.0.CO;2-K.
- [6] Beauchemin, C. A. A., McSharry, J. J., Drusano, G. L., Nguyen, J. T., Went, G. T., Ribeiro, R. M., & Perelson, A. S. (2008). Modeling amantadine treatment of influenza A virus in vitro. *J. Theor. Biol.*, *254*, 439–451. doi:10.1016/j.jtbi.2008.05.031.
- [7] Benton, K. A., Mispion, J. A., Lo, C. Y., Brutkiewicz, R. R., Prasad, S. A., & Epstein, S. L. (2001). Heterosubtypic immunity to influenza A virus in mice lacking IgA, all Ig, NKT cells, or gamma delta T cells. *J. Immunol.*, *166*, 7437–7445. doi:10.4049/jimmunol.166.12.7437.
- [8] Bocharov, G. A., & Romanyukha, A. A. (1994). Mathematical model of antiviral immune response III. Influenza A virus infection. *J. Theor. Biol.*, *167*, 323–360.
- [9] Bortnick, A., & Allman, D. (2013). What is and what should always have been: long-lived plasma cells induced by T cell-independent antigens. *J. Immunol.*, *190*, 5913–5918. doi:10.4049/jimmunol.1300161.
- [10] Butler, J., Hooper, K. A., Petrie, S., Lee, R., Maurer-Stroh, S., Reh, L., Guarnaccia, T., Baas, C., Xue, L., Vitesnik, S., Leang, S.-K., McVernon, J., Kelso, A., Barr, I. G., McCaw, J. M., Bloom, J. D., & Hurt, A. C. (2014). Estimating the fitness advantage conferred by permissive neuraminidase mutations in recent oseltamivir-resistant A(H1N1)pdm09 influenza viruses. *PLoS Pathog.*, *10*, e1004065. doi:10.1371/journal.ppat.1004065.
- [11] Cao, P., Wang, Z., Yan, A. W. C., McVernon, J., Xu, J., Heffernan, J. M., Kedzierska, K., & McCaw, J. M. (2016). On the role of CD8+ T cells in determining recovery time from influenza virus infection. *Front. Immunol.*, *7*, 611. doi:10.3389/fimmu.2016.00611.

- [12] Cao, P., Yan, A. W. C., Heffernan, J. M., Petrie, S., Moss, R. G., Carolan, L. A., Guarnaccia, T. A., Kelso, A., Barr, I. G., McVernon, J., Laurie, K. L., & McCaw, J. M. (2015). Innate immunity and the inter-exposure interval determine the dynamics of secondary influenza virus infection and explain observed viral hierarchies. *PLoS Comput. Biol.*, *11*, e1004334. doi:10.1371/journal.pcbi.1004334.
- [13] Chang, D. B., & Young, C. S. (2007). Simple scaling laws for influenza A rise time, duration, and severity. *J. Theor. Biol.*, *246*, 621–635. doi:10.1016/j.jtbi.2007.02.004.
- [14] Chao, D. L., Davenport, M. P., Forrest, S., & Perelson, A. S. (2004). A stochastic model of cytotoxic T cell responses. *J. Theor. Biol.*, *228*, 227–240. doi:10.1016/j.jtbi.2003.12.011.
- [15] Cohen, S. D., Hindmarsh, A. C., & Dubois, P. F. (1996). CVODE, a stiff/nonstiff ODE solver in C. *Computers in Physics*, *10*, 138–148. doi:10.1063/1.4822377.
- [16] Davenport, M. P., Fazou, C., McMichael, A. J., & Callan, M. F. C. (2002). Clonal selection, clonal senescence, and clonal succession: the evolution of the T cell response to infection with a persistent virus. *J. Immunol.*, *168*, 3309–17. doi:10.4049/jimmunol.168.7.3309.
- [17] De Boer, R. J., Oprea, M., Antia, R., Murali-Krishna, K., Ahmed, R., & Perelson, A. S. (2001). Recruitment times, proliferation, and apoptosis rates during the CD8+ T-cell response to lymphocytic choriomeningitis virus. *J. Virol.*, *75*, 10663–10669. doi:10.1128/JVI.75.22.10663-10669.2001.
- [18] Dobrovolny, H. M., Reddy, M. B., Kamal, M. A., Rayner, C. R., & Beauchemin, C. A. A. (2013). Assessing mathematical models of influenza infections using features of the immune response. *PLoS ONE*, *8*, e57088. doi:10.1371/journal.pone.0057088.
- [19] Earl, D. J., & Deem, M. W. (2005). Parallel tempering: theory, applications, and new perspectives. *Phys. Chem. Chem. Phys.*, *7*, 3910–3916. doi:10.1039/B509983H.
- [20] Epstein, J. M., Goedecke, D. M., Yu, F., Morris, R. J., Wagener, D. K., & Bobashev, G. V. (2007). Controlling pandemic flu: The value of international air travel restrictions. *PLoS ONE*, *2*. doi:10.1371/journal.pone.0000401.

- [21] Gelman, A., Carlin, J. B., Stern, H. S., & Rubin, D. B. (2004). *Bayesian Data Analysis*. (2nd ed.). London, UK: Chapman & Hall/CRC.
- [22] Gelman, A., Roberts, G. O., & Gilks, W. R. (1995). Efficient metropolis jumping rules. In J. M. Bernardo, J. O. Berger, A. P. Dawid, & A. F. M. Smith (Eds.), *Bayesian Statistics 5* (pp. 599–607). New York: Oxford University Press.
- [23] Gelman, A., & Rubin, D. B. (1992). Inference from iterative simulation using multiple sequences. *Stat. Sci.*, *7*, 457–472.
- [24] Geman, S., & Geman, D. (1984). Stochastic relaxation, Gibbs distributions, and the Bayesian restoration of images. *IEEE Trans. Pattern Anal. Mach. Intell.*, *PAMI-6*, 721–741. doi:10.1109/TPAMI.1984.4767596.
- [25] Geyer, C. J. (1991). Markov chain Monte Carlo maximum likelihood. In *Computing Science and Statistics: Proceedings of the 23rd Symposium on the Interface* (p. 156). Interface Foundation of North America.
- [26] Grebe, K. M., Yewdell, J. W., & Bennink, J. R. (2008). Heterosubtypic immunity to influenza A virus: where do we stand? *Microb. Infect.*, *10*, 1024–9. doi:10.1016/j.micinf.2008.07.002.
- [27] Hancioglu, B., Swigon, D., & Clermont, G. (2007). A dynamical model of human immune response to influenza A virus infection. *J. Theor. Biol.*, *246*, 70–86. doi:10.1016/j.jtbi.2006.12.015.
- [28] Handel, A., Longini Jr, I. M., & Antia, R. (2007). Neuraminidase inhibitor resistance in influenza: assessing the danger of its generation and spread. *PLoS Comput. Biol.*, *3*, e240. doi:10.1371/journal.pcbi.0030240.
- [29] Handel, A., Longini Jr, I. M., & Antia, R. (2010). Towards a quantitative understanding of the within-host dynamics of influenza A infections. *J. R. Soc. Interface*, *7*, 35–47. doi:10.1098/rsif.2009.0067.
- [30] Heffernan, J. M., & Keeling, M. J. (2008). An in-host model of acute infection: measles as a case study. *Theor. Popul. Biol.*, *73*, 134–147. doi:10.1016/j.tpb.2007.10.003.
- [31] Heffernan, J. M., Smith, R. J., & Wahl, L. M. (2005). Perspectives on the basic reproductive ratio. *J. R. Soc. Interface*, *2*, 281–293. doi:10.1098/rsif.2005.0042.

- [32] Iwasaki, T., & Nozima, T. (1977). Defense mechanisms against primary influenza virus infection in mice I. The roles of interferon and neutralizing antibodies and thymus dependence of interferon and antibody production. *J. Immunol.*, *118*, 256–263.
- [33] John W. Eaton, S. H., David Bateman, & Wehbring, R. (2014). *GNU Octave version 3.8.1 manual: a high-level interactive language for numerical computations*. CreateSpace Independent Publishing Platform. URL: <http://www.gnu.org/software/octave/doc/interpreter> ISBN 1441413006.
- [34] Kaech, S. M., & Ahmed, R. (2001). Memory CD8+ T cell differentiation: initial antigen encounter triggers a developmental program in naïve cells. *Nat. Immunol.*, *2*, 415–22. doi:10.1038/87720.
- [35] Kaech, S. M., Hemby, S., Kersh, E., & Ahmed, R. (2002). Molecular and functional profiling of memory CD8 T cell differentiation. *Cell*, *111*, 837–851. doi:10.1016/s0092-8674(02)01139-x.
- [36] Kone, A., & Kofke, D. A. (2005). Selection of temperature intervals for parallel-tempering simulations. *J. Chem. Phys.*, *122*, 206101. doi:10.1063/1.1917749.
- [37] Kris, R. M., Yetter, R. A., Cogliano, R., Ramphal, R., & Small, P. A. (1988). Passive serum antibody causes temporary recovery from influenza virus infection of the nose, trachea and lung of nude mice. *Immunology*, *63*, 349–53.
- [38] Laurie, K. L., Guarnaccia, T. A., Carolan, L. A., Yan, A. W. C., Aban, M., Petrie, S., Cao, P., Heffernan, J. M., McVernon, J., Mosse, J., Kelso, A., McCaw, J. M., & Barr, I. G. (2015). Interval between infections and viral hierarchy are determinants of viral interference following influenza virus infection in a ferret model. *J. Infect. Dis.*, *212*, 1701–1710. doi:10.1093/infdis/jiv260.
- [39] Lee, H. Y., Topham, D. J., Park, S. Y., Hollenbaugh, J., Treanor, J., Mosmann, T. R., Jin, X., Ward, B. M., Miao, H., Holden-Wiltse, J., Perelson, A. S., Zand, M., & Wu, H. (2009). Simulation and prediction of the adaptive immune response to influenza A virus infection. *J. Virol.*, *83*, 7151–7165. doi:10.1128/JVI.00098-09.
- [40] Lehmann-Grube, F., Assmann, U., Löliger, C., Moskophidis, D., & Löhler, J. (1985). Mechanism of recovery from acute virus infection.

- I. Role of T lymphocytes in the clearance of lymphocytic choriomeningitis virus from spleens of mice. *J. Immunol.*, *134*, 608–15.
- [41] Li, Y., & Handel, A. (2014). Modeling inoculum dose dependent patterns of acute virus infections. *J. Theor. Biol.*, *347*, 63–73. doi:10.1016/j.jtbi.2014.01.008.
- [42] Marchuk, G. I., Petrov, R. V., Romanyukha, A. A., & Bocharov, G. A. (1991). Mathematical model of antiviral immune response. I. Data analysis, generalized picture construction and parameters evaluation for hepatitis B. *J. Theor. Biol.*, *151*, 1–40. doi:10.1016/S0022-5193(05)80142-0.
- [43] Marriott, A. C., & Dimmock, N. J. (2010). Defective interfering viruses and their potential as antiviral agents. *Rev. Med. Virol.*, *20*, 51–62. doi:10.1002/rmv.641.
- [44] MATLAB (2015). *R2015b*. Natick, Massachusetts: The MathWorks Inc.
- [45] Metropolis, N., Rosenbluth, A. W., Rosenbluth, M. N., Teller, A. H., & Teller, E. (1953). Equation of state calculations by fast computing machines. *J. Chem. Phys.*, *21*, 1087–1092. doi:10.1063/1.1699114.
- [46] Metropolis, N., & Ulam, S. (1949). The Monte Carlo method. *JASA*, *44*, 335–341. doi:10.1080/01621459.1949.10483310.
- [47] Miao, H., Hollenbaugh, J. A., Zand, M. S., Holden-Wiltse, J., Mosmann, T. R., Perelson, A. S., Wu, H., & Topham, D. J. (2010). Quantifying the early immune response and adaptive immune response kinetics in mice infected with influenza A virus. *J. Virol.*, *84*, 6687–6698. doi:10.1128/JVI.00266-10.
- [48] Mingos Wols, H. A. (2015). Plasma Cells. In *eLS 2006* (pp. 1–11). Chichester, UK: John Wiley & Sons, Ltd. doi:10.1002/9780470015902.a0004030.pub2.
- [49] Mitchell, H., Levin, D., Forrest, S., Beauchemin, C. A. A., Tipper, J., Knight, J., Donart, N., Layton, R. C., Pyles, J., Gao, P., Harrod, K. S., Perelson, A. S., & Koster, F. (2011). Higher level of replication efficiency of 2009 (H1N1) pandemic influenza virus than those of seasonal and avian strains: kinetics from epithelial cell culture and computational modeling. *J. Virol.*, *85*, 1125–35. doi:10.1128/JVI.01722-10.

- [50] Möhler, L., Flockerzi, D., Sann, H., & Reichl, U. (2005). Mathematical model of influenza A virus production in large-scale microcarrier culture. *Biotechnol. Bioeng.*, *90*, 46–58. doi:10.1002/bit.20363.
- [51] Murali-Krishna, K., Altman, J. D., Suresh, M., Sourdive, D. J., Zajac, A. J., Miller, J. D., Slansky, J., & Ahmed, R. (1998). Counting antigen-specific CD8 T cells: a reevaluation of bystander activation during viral infection. *Immunity*, *8*, 177–87. doi:10.1016/S1074-7613(00)80470-7.
- [52] Nayak, D. P., Chambers, T. M., & Akkina, R. K. (1985). Defective-interfering (di) RNAs of influenza viruses: origin, structure, expression, and interference. In M. Cooper, H. Eisen, W. Goebel, P. H. Hofschneider, H. Koprowski, F. Melchers, M. Oldstone, R. Rott, H. G. Schweiger, P. K. Vogt, & I. Wilson (Eds.), *Current Topics in Microbiology and Immunology* (pp. 103–151). Berlin, Heidelberg: Springer Berlin Heidelberg. doi:10.1007/978-3-642-70227-3_3.
- [53] Nowak, M. A., Lloyd, A. L., Vasquez, G. M., Wiltrout, T. A., Wahl, L. M., Bischofberger, N., Williams, J., Kinter, A., Fauci, A. S., Hirsch, V. M., & Lifson, J. D. (1997). Viral dynamics of primary viremia and antiretroviral therapy in simian immunodeficiency virus infection. *J. Virol.*, *71*, 7518–25.
- [54] Paradis, E. G., Pinilla, L. T., Holder, B. P., Abed, Y., Boivin, G., & Beauchemin, C. A. A. (2015). Impact of the H275Y and I223V mutations in the neuraminidase of the 2009 pandemic influenza virus in vitro and evaluating experimental reproducibility. *PLoS ONE*, *10*, e0126115. doi:10.1371/journal.pone.0126115.
- [55] Pawelek, K. A., Huynh, G. T., Quinlivan, M., Cullinane, A., Rong, L., & Perelson, A. S. (2012). Modeling within-host dynamics of influenza virus infection including immune responses. *PLoS Comput. Biol.*, *8*, e1002588. doi:10.1371/journal.pcbi.1002588.
- [56] Petrie, S. M., Butler, J., Barr, I. G., McVernon, J., Hurt, A. C., & McCaw, J. M. (2015). Quantifying relative within-host replication fitness in influenza virus competition experiments. *J. Theor. Biol.*, *382*, 259–271. doi:10.1016/j.jtbi.2015.07.003.
- [57] Petrie, S. M., Guarnaccia, T., Laurie, K. L., Hurt, A. C., McVernon, J., & McCaw, J. M. (2013). Reducing uncertainty in within-host parameter estimates of influenza infection by measuring both infectious and

- total viral load. *PLoS ONE*, 8, e64098. doi:10.1371/journal.pone.0064098.
- [58] Pinilla, L. T., Holder, B. P., Abed, Y., Boivin, G., & Beauchemin, C. A. A. (2012). The H275Y neuraminidase mutation of the pandemic A/H1N1 influenza virus lengthens the eclipse phase and reduces viral output of infected cells, potentially compromising fitness in ferrets. *J. Virol.*, 86, 10651–10660. doi:10.1128/JVI.07244-11.
- [59] Plummer, M., Best, N., Cowles, K., & Vines, K. (2006). CODA: convergence diagnosis and output analysis for MCMC. *R News*, 6, 7–11.
- [60] R Core Team (2016). *R: A Language and Environment for Statistical Computing*. R Foundation for Statistical Computing Vienna, Austria. URL: <https://www.R-project.org/>.
- [61] Rathore, N., Chopra, M., & De Pablo, J. J. (2005). Optimal allocation of replicas in parallel tempering simulations. *J. Chem. Phys.*, 122, 024111. doi:10.1063/1.1831273.
- [62] Raue, A., Kreutz, C., Maiwald, T., Bachmann, J., Schilling, M., Klingmüller, U., & Timmer, J. (2009). Structural and practical identifiability analysis of partially observed dynamical models by exploiting the profile likelihood. *Bioinformatics*, 25, 1923–1929. doi:10.1093/bioinformatics/btp358.
- [63] Saenz, R. A., Quinlivan, M., Elton, D., MacRae, S., Blunden, A. S., Mumford, J. A., Daly, J. M., Digard, P., Cullinane, A., Grenfell, B. T., McCauley, J. W., Wood, J. L. N., & Gog, J. R. (2010). Dynamics of influenza virus infection and pathology. *J. Virol.*, 84, 3974–3983. doi:10.1128/JVI.02078-09.
- [64] Seo, S. H., Hoffmann, E., & Webster, R. G. (2002). Lethal H5N1 influenza viruses escape host anti-viral cytokine responses. *Nat. Med.*, 8, 950–4. doi:10.1038/nm757.
- [65] Smith, A. M., & Perelson, A. S. (2011). Influenza A virus infection kinetics: quantitative data and models. *Wiley Interdiscip. Rev. Syst. Biol. Med.*, 3, 429–445. doi:10.1002/wsbm.129.
- [66] van Stipdonk, M. J. B., Lemmens, E. E., & Schoenberger, S. P. (2001). Naïve CTLs require a single brief period of antigenic stimulation for clonal expansion and differentiation. *Nat. Immunol.*, 2, 423–429. doi:10.1038/87730.

- [67] Sze, D. M.-Y., Toellner, K.-M., García de Vinuesa, C., Taylor, D. R., & MacLennan, I. C. M. (2000). Intrinsic constraint on plasmablast growth and extrinsic limits of plasma cell survival. *J. Exp. Med.*, *192*, 813–821. doi:10.1084/jem.192.6.813.
- [68] Terajima, M., Babon, J. A. B., Co, M. D. T., & Ennis, F. A. (2013). Cross-reactive human B cell and T cell epitopes between influenza A and B viruses. *Viol. J.*, *10*, 244. doi:10.1186/1743-422X-10-244.
- [69] Vanlier, J., Tiemann, C. A., Hilbers, P. A. J., & van Riel, N. A. W. (2012). A Bayesian approach to targeted experiment design. *Bioinformatics*, *28*, 1136–1142. doi:10.1093/bioinformatics/bts092.
- [70] Veiga-Fernandes, H., Walter, U., Bourgeois, C., McLean, A., & Rocha, B. (2000). Response of naïve and memory CD8+ T cells to antigen stimulation in vivo. *Nat. Immunol.*, *1*, 47–53. doi:10.1038/76907.
- [71] Wodarz, D., & Thomsen, A. R. (2005). Does programmed CTL proliferation optimize virus control? *Trends Immunol.*, *26*, 305–310. doi:10.1016/j.it.2005.04.007.
- [72] Yan, A. W. C., Cao, P., Heffernan, J. M., McVernon, J., Quinn, K. M., La Gruta, N. L., Laurie, K. L., & McCaw, J. M. (2017). Modelling cross-reactivity and memory in the cellular adaptive immune response to influenza infection in the host. *J. Theor. Biol.*, *413*, 34–49. doi:10.1016/j.jtbi.2016.11.008.
- [73] Yan, A. W. C., Cao, P., & McCaw, J. M. (2016). On the extinction probability in models of within-host infection: the role of latency and immunity. *J. Math. Biol.*, *73*, 787–813. doi:10.1007/s00285-015-0961-5.
- [74] Yap, K. L., & Ada, G. L. (1978). Cytotoxic T cells in the lungs of mice infected with an influenza A virus. *Scand. J. Immunol.*, *7*, 73–80. doi:10.1111/j.1365-3083.1978.tb00428.x.